JOURNAL OF PETROLOGY | VOLUME 43 | NUMBER 2 | PAGES 345–373 | 2002

Kistufell: Primitive Melt from the Iceland Mantle Plume

KRESTEN BREDDAM*

NORDIC VOLCANOLOGICAL INSTITUTE, GRENSÁSVEGUR 50, 108 REYKJAVIK, ICELAND
DANISH LITHOSPHERE CENTRE, ØSTER VOLDGADE 10L, DK-1350, COPENHAGEN K, DENMARK

RECEIVED NOVEMBER 4, 1998; REVISED TYPESCRIPT ACCEPTED AUGUST 24, 2001

This paper presents new geochemical data from Kistufell (64°48′N, 17°13′W), a monogenetic table mountain situated directly above the inferred locus of the Iceland mantle plume. Kistufell is composed of the most primitive olivine tholeiitic glasses found in central Iceland (MgO 10·56 wt %, olivine $Fo_{89·7}$). The glasses are interpreted as near-primary, high-degree plume melts derived from a heterogeneous mantle source. Mineral, glass and bulk-rock (glass + minerals) chemistry indicates a low average melting pressure (15 kbar), high initial crystallization pressures and temperatures (10–15 kbar and 1270°C), and eruption temperatures (1240°C) that are among the highest observed in Iceland. The glasses have trace element signatures (La_n/Yb_n <1, Ba_n/Zr_n 0·55–0·58) indicative of a trace element depleted source, and the Sr–Nd–Pb isotopic ratios ($^{87}Sr/^{86}Sr$ 0·70304–0·70308, $^{143}Nd/^{144}Nd$ 0·513058–0·513099, $^{206}Pb/^{204}Pb$ 18·343–18·361) further suggest a long-term trace element depletion relative to primordial mantle. High He isotopic ratios (15·3–16·8 R/R_a) combined with low $^{207}Pb/^{204}Pb$ (15·42–15·43) suggest that the mantle source of the magma is different from that of North Atlantic mid-ocean ridge basalt. Negative Pb anomalies, and positive Nb and Ta anomalies indicate that the source includes a recycled, subducted oceanic crustal or mantle component. Positive Sr anomalies (Sr_n/Nd_n = 1·39–1·50) further suggest that this recycled source component involves lower oceanic crustal gabbros. The $\delta^{18}O$ values (4·2–4·7‰), which are lower than those observed in mantle peridotites but similar to those observed in ophiolites and in situ *oceanic gabbros, are consistent with this interpretation. The elevated $^3He/^4He$ ratios are primarily attributed to a primitive, relatively undegassed component in the Iceland mantle plume, which dominates the He isotope signature as a result of long-term depletion of U, Th and He in the recycled gabbroic component.*

KEY WORDS: *isotopes; Iceland plume; primitive basalts; recycled oceanic lithosphere*

INTRODUCTION

Iceland is the surface manifestation of a plume of actively upwelling mantle superimposed on a mid-ocean ridge. The Icelandic crust is distinctive for its anomalous thickness (Darbyshire *et al.*, 2000) and its significant petrological and geochemical variations relative to the adjacent sectors of the mid-ocean ridge (e.g. Taylor *et al.*, 1997). These features are generally ascribed to active upwelling and melting of anomalously hot mantle material that is compositionally different from that of the surrounding upper mantle (e.g. Ito *et al.*, 1999; Chauvel & Hemond, 2000). The nature of the individual source components within the plume remains, however, enigmatic.

The most compelling evidence for involvement of a lower-mantle plume component are the high $^3He/^4He$ ratios (up to 37 R/R_a, Hilton *et al.*, 1999) (R/R_a is the ratio of $^3He/^4He$ in the sample relative to that in the atmosphere). This is well outside the variation in the global ridge system (9·13 ± 3·57 R/R_a, Anderson, 2000) and a feasible explanation is derivation from relatively undegassed mantle material hitherto isolated at depth (Kurz *et al.*, 1985; Hilton *et al.*, 1999; Breddam *et al.*, 2000). Incompatible trace element rich, high $^{87}Sr/^{86}Sr$ and $^{206}Pb/^{204}Pb$, and low $^{143}Nd/^{144}Nd$ 'enriched' Icelandic lavas have also been attributed to an inherent plume component, which could either be (high $^3He/^4He$) lower mantle (e.g. Hanan *et al.*, 2000; Kempton *et al.*, 2000) or recycled oceanic basalts (Chauvel & Hemond, 2000). However, the relation between the plume and the material giving rise to incompatible trace element poor, low $^{87}Sr/^{86}Sr$ and $^{206}Pb/^{204}Pb$, and high $^{143}Nd/^{144}Nd$ 'depleted' Icelandic lavas is more controversial (Chauvel & Hemond, 2000; Hanan *et al.*, 2000; Kempton *et al.*, 2000). The question is whether this depleted material is (1) an

*Present address: Danish Lithosphere Centre, Øster Voldgade 10L, DK-1350, Copenhagen K, Denmark. Telephone: (+45) 38142653. Fax: (+45) 33110878. E-mail: kbd@dlc.ku.dk

intrinsic plume component or (2) the source of North Atlantic normal mid-ocean ridge basalt (N-MORB) upwelling along the Mid-Atlantic spreading centre and possibly entrained in the plume.

The answer is closely tied to the interpretation of a few geochemical features; most importantly, excess Sr, ^{18}O-depletion and low ^{207}Pb/^{204}Pb, which distinguish depleted Icelandic lavas from North Atlantic N-MORB (Hemond *et al.* 1993; Chauvel & Hemond, 2000). Identifying the source of these geochemical anomalies is not trivial, however. Although excess Sr and ^{18}O-depletion in other ocean-island basalts (OIB) have been attributed to recycled oceanic crust in their mantle source (Lassiter & Hauri, 1998; Sobolev *et al.*, 2000), a similar interpretation is not obvious for Iceland. This is because interaction between North Atlantic N-MORB and local hydrothermally altered crust can produce similar geochemical anomalies in Icelandic basalts (Hemond *et al.*, 1993). Such contamination processes, on the other hand, cannot explain why depleted Icelandic lavas apparently have lower ^{207}Pb/^{204}Pb ratios than most North Atlantic N-MORB (Hards *et al.*, 1995; Thirlwall, 1995). On this basis, depleted Icelandic lavas have been associated with an intrinsic plume source distinct from the ambient upper mantle (Kerr *et al.*, 1995). The observation was, however, questioned by Mertz & Haase (1997), who used a broader Pb isotope dataset to show a complete overlap between Icelandic basalts and North Atlantic N-MORB. Also, errors in mass fractionation correction may have led to misinterpretations of Pb isotope measurements, as recently pointed out by Thirlwall (2000).

The present paper explores the origin of depleted basalts erupted at Kistufell, directly above the inferred axis of the Iceland mantle plume (Wolfe *et al.*, 1997). It presents a detailed account of the geochemistry of the most primitive ol-tholeiitic glasses found in central Iceland, and further examines the sources of excess Sr and ^{18}O-depletion. Following previous investigations of melting dynamics and mantle sources beneath Iceland (Elliott *et al.*, 1991; Thirlwall, 1995; Slater *et al.*, 1998, 2001; Stracke *et al.*, 1998), the study focuses on unusually MgO-rich ol-tholeiites to minimize potential contamination problems. The previous studies, however, were mainly concerned with lavas from the southernmost and northernmost extremities of the neovolcanic rift zone in Iceland (Reykjanes and Theystareykir, respectively) most distant from the plume axis. These spreading sectors are characterized by relatively thin crust (<20 km) compared with the 30–40 km (Darbyshire *et al.*, 2000) above the inferred plume axis in SE Iceland. This could affect both the minimum depth of melting and the average crustal residence times and thereby the composition of the lavas (Gurenko & Chaussidon, 1995; Gee *et al.*, 1998*a*). The differences in setting could also be important because the southernmost and northernmost sectors of the neovolcanic rift zone are distal to the plume axis and may be prone to shallow-level influx of ambient upper-mantle material as suggested by Mertz *et al.* (1991). This study suggests that the depleted Kistufell basalts are unrelated to ambient upper mantle. It further shows that the magmas passed the crust virtually uncontaminated. When combined with previously published data for Icelandic basalts and North Atlantic MORB, these new results support the hypothesis that one source component of the depleted Icelandic lavas is recycled oceanic gabbros (Chauvel & Hemond, 2000).

GEOLOGICAL SETTING OF KISTUFELL AND SAMPLE DETAILS

Kistufell (64°48′N, 17°13′W) is a previously uninvestigated monogenetic table mountain located in the neovolcanic northern rift zone (NRZ) at the NW margin of the Vatnajökull ice cap (Fig. 1). The central axis of the plume is thought to be located below this region, which is at present the locus of maximum eruption frequency, maximum crustal accretion (Jakobsson, 1979; Larsen *et al.*, 1998), and maximum perturbations of gravity (–55 mGal) and seismic velocity (–4%) (Eysteinsson & Gunnarsson, 1995; Wolfe *et al.*, 1997). The exposed volume of Kistufell is estimated here at $\sim$1 km^3. The original volume of Kistufell is difficult to estimate, however, as the volume lost through glacial erosion is uncertain, and because postglacial lavas obscure the base of the structure. Kistufell consists of a major, lower sequence of subglacially erupted pillow lavas, hyaloclastites, and occasional breccias, capped by a minor sequence of subaerially erupted lavas. The sampled eastern and northern flanks are dominated by coalesced pillow mounds and hyaloclastite aprons, respectively. The western flank and southern flank are covered by sediments and ice and have not been sampled. Abundant tectonic and volcanic lineaments, NE–SW-oriented hyaloclastite ridges, and late-stage explosion craters across Kistufell indicate the existence of underlying fissures or faults, which may have acted as magma conduits.

The precise age of Kistufell is not known. However, Kistufell is a relatively small table mountain compared with the more prominent table mountains in the NRZ (e.g. Herdubreid: Werner, 1994), and it is argued below that it formed when the icecap was relatively thin. An assessment of the thickness of the icecap at the time of eruption requires an estimation of the depth to the base of the structure, which is now obscured by postglacial lavas. The average thickness of postglacial basalts is 36–42 m, judged from the postglacial productivity of volcanic systems above the inferred plume stem (3·6 and 4·2 km^3/100 km^2) for Grimsvötn and Veidivötn, respectively (Jakobsson, 1979). Therefore, unless (1) the

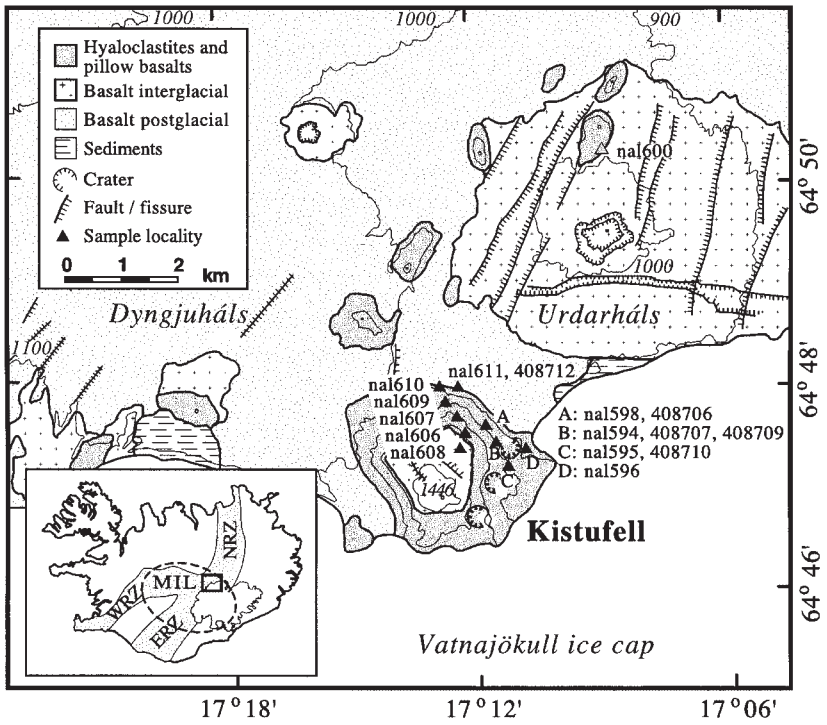

Fig. 1. Schematic map of the Kistufell region compiled from unpublished geological maps and Gudmundsson (1996). Lithology includes intraglacial and postglacial eruptive units. Sample localities are marked by filled triangles (Kistufell: black). The tectonic lineaments through Urdarháls that are oriented towards Kistufell should be noted: the hyaloclastite ridge (nal600: grey triangle) at the northern end of the graben structure is geochemically similar to Kistufell (see Fig. 6b). Spot and contour line elevations (in italics) are given in metres. The insert outlines the rift zones of Iceland (grey), icecaps (outline + white), the study area (box), and position and lateral dimensions of seismic low-velocity anomaly (broken line) by Wolfe *et al.* (1997). NRZ, Northern Rift Zone; ERZ, Eastern Rift Zone; WRZ, Western Rift Zone; MIL, Mid-Iceland Belt.

local productivity was considerably different or (2) postglacial lavas accumulated particularly around Kistufell, the depth to the base is <50 m. As the Kistufell subaerial lavas occur ~350 m above the current surrounding plain, the thickness of the structure can therefore be judged to have been roughly 400 m when the subaerial lavas started to form. With reference to the 1996 subglacial Gjálp eruption, which became subaerial in a roughly 200 m deep depression in the icecap, it can be assumed that at least a similar depression formed in the local icecap during the Kistufell eruption. The actual icecap thickness can thus be judged to have been ~600–700 m, which is considerably reduced relative to the peak thickness of the Weichselian icecap (1000–1500 m) (Walker, 1965; Bourgeois *et al.*, 1998). Kistufell is therefore suggested to have formed towards the end of the glaciation when considerable amounts of ice had disappeared.

The high eruption frequency of picrites and ol-tholeiites in early postglacial times (Jakobsson *et al.*, 1978) has inspired the idea that decreasing iceload (lithostatic pressure) during the early Holocene caused crustal rebound, which led to further mantle decompression, higher melt fractions and increased lava extrusion rates (Hardarson & Fitton, 1991; Sigvaldason *et al.*, 1992; Jull & McKenzie 1996; Slater *et al.*, 1998). It is suggested here that crustal rebound led to differential movement of crustal blocks within the pre-existing tectonic framework and thereby facilitated extrusion of the Kistufell magma. This idea is substantiated by the fact that a hyaloclastite ridge (nal600) located 6 km to the NNE on a local tectonic lineament oriented towards Kistufell (Fig. 1) is compositionally completely identical to Kistufell (see Fig. 6b, below). The point is important, because it illustrates that the decreasing iceload in Iceland, besides causing the generation of high melt fractions, indirectly may have facilitated magma transport and led to reduced crustal residence times for late glacial and postglacial magmas, as previously inferred by Gee *et al.* (1998*a*).

Fresh basalts, pillow rims and hyaloclastites from the northern and eastern flanks of Kistufell, and from a hyaloclastite ridge (nal600) (Fig. 1) were analysed as part of this study. Pillow basalts or rims have been collected from separate flows near the base of the main structure (408706, 408712), and from pillow mounds thought to be related to a single flow located on the eastern flank of Kistufell (locations B, C and D, Fig. 1). As shown

below, the rocks generally have very similar compositions: the variation of Sr, Nd, Pb and O isotope ratios is within the analytical error and major and trace element variations are slightly outside the analytical error, mainly as a result of varying amounts of phenocrysts. Kistufell is therefore believed to be monogenetic and to have erupted from a reservoir that did not fractionate during the period of emplacement. The Kistufell hyaloclastites are subglacially erupted, essentially subaquatic sedimentary rocks composed of innumerable individual glass shards, formed by quenching of magma in contact with water. They have not suffered post-eruptive fractionation, as is often the case with basaltic lavas or pillows, and therefore, fresh glass shards from the hyaloclastites represent the closest approximation to the erupted magma composition.

ANALYTICAL TECHNIQUES

A total of 20 samples including pillow rim glasses ($n = 9$), hyaloclastite glasses ($n = 7$), pillow basalts ($n = 3$) and a basalt flow capping Kistufell ($n = 1$) have been analysed in this study. All of the glass analyses were carried out on handpicked fragments or shards without secondary fillings in vesicles, as hydration of basaltic glasses usually leads to considerable leaching of SiO_2, Al_2O_3, CaO, Na_2O, K_2O, Rb, Ba, and Sr in addition to oxidation of iron (Jakobsson, 1971; Furnes, 1974, 1975). The collected pillow rim fragments were completely vitreous on all sides. The fractions of handpicked pillow rim glass fragments and hyaloclastite glass shards are considered to be unaffected by secondary alteration because (1) electron microprobe analysis of different fragments or shards gave identical compositions (within analytical uncertainty) and (2) iron is in an extremely reduced state relative to Icelandic basalts in general (see below).

Mineral and glass compositional data were obtained using an ARL SEMQ electron microprobe at the Nordic Volcanological Institute (Tables 1–4). The acceleration voltage was 15 kV, and the beam current was 25–30 nA for olivine, Cr-spinel and plagioclase, and 15 nA for glass. The counting time was generally 20 s for each element, except for mineral traverses (10 s) and Ni in olivine (60 s). Typical analytical precision, calculated from repeated analyses of a homogeneous basaltic glass (nal611), is $<\pm 2\%$ for SiO_2, Al_2O_3, FeO and CaO; ± 2–5% for MgO, Na_2O and TiO_2; ± 5–15% for K_2O; and >15% for MnO and P_2O_5. This means that, for example, plagioclase compositions are estimated to a precision of typically $\pm 0{\cdot}1$ An%. Analyses summing to <98 wt % or with large deviation from the appropriate stoichiometric cation totals were not accepted. Mössbauer Fe^{3+}/Fe^{tot} spectroscopy was carried out at the Science Institute, University of Iceland, on three of the handpicked glass samples (nal595, nal600 and nal611), powdered in an agate mortar under propanol. The spectra were recorded on a conventional accelerator spectrometer (room temperature) and fitted with two broad line doublets for ferrous iron and one doublet for ferric iron, which is sufficient to determine Fe^{3+}/Fe^{tot} to within 3% (Helgason & Steinthorsson, 1989). This method is particularly well suited for high-MgO glasses as it resolves the ferric/ferrous iron ratio in olivine microcrystallites in addition to the amorphous glass [details have been given by Oskarsson *et al.* (1994)].

Whole-rock major element compositions (and Cr) (Table 5) of glasses and basalts were analysed by inductively coupled plasma atomic emission spectroscopy (ICP-AES) at the Nordic Volcanological Institute, using a Thermo-Jarell Ash Atomscan 25 ICP spectrometer after fusion in graphite crucibles (1000°C) of 500 mg of sample (crushed in agate) with 1500 mg $LiBO_2$ and dissolution in HNO_3–HCl–oxalate mixture. All elements were analysed at 1150 V, except Na (950 V). To eliminate time-dependent fluctuations in sample introduction and nebulization, silica in the sample was used as an internal standard: all other elements were calibrated based on their radiant intensities relative to that of silica. The analysis is thus based on intensity ratio measurements rather than absolute intensities. Absolute abundances are based on recalculation to 100%. The analytical precision is better than 3% based on duplicate analyses of homogeneous glass. All other trace elements (except Cr) were analysed by inductively coupled plasma mass spectrometry (ICP-MS) (CNRS, SARM, Vandoeuvre, France) after fusion of samples in $LiBO_2$ and HNO_3 dissolution. BTHO (split of BIR-1) was analysed as external standard. The precision is $<\pm 5\%$ for La, Gd, Ho, Yb, Lu, Sr, Sc, Co, Zn and Zr; ± 5–10% for Y, Ce, Pr, Nd, Sm, Eu, Tb and Tm; ± 10–15% for Cu, Dy, Er and Ta; and ± 15–20% for Ni, Nb, Rb and Ba. However, the precision is probably better than $\pm 10\%$ for Nb, Ta, Rb and Ba, as these elements are typically four times more abundant in the samples relative to the standard.

A subset of glasses (408706–408712, Geological Survey of Denmark and Greenland number series) were analysed for major element, trace element and isotopic compositions by direct acid-digestion, avoiding any form of crushing and thereby potential contamination from the crushing equipment. Major elements for the subset were analysed by X-ray fluorescence (XRF) on fused glass discs of handpicked glass separates with $Na_2B_4O_7$-flux using a Phillips PW1606 (Na_2O determined by atomic absorption spectroscopy (AAS) using a Perkin Elmer PE2280 and FeO by wet titration (details have been given by Kystol & Larsen (1999)]. Trace elements in the same subset of glasses were analysed by ICP-MS, using

Table 1: Representative electron microprobe analyses of olivine

Sample:	nal594	nal594	nal595	nal595	nal598	nal598	nal606	nal606	nal607
Location:	Kistufell	Kistufell	Kistufell	Kistufell	Kistufell	Kistufell	Kistufell	Kistufell	Kistufell
Size (mm):	0·17	0·34	1·00	0·27	0·02	0·02	0·90	0·02	0·08
ID:	ol1/c	ol2/r	ol2/c	ol1/r	ol2/c	ol3/c	ol1/r	ol5/c	ol3/c
wt %									
SiO_2	40·24	39·46	40·79	39·80	40·51	39·59	39·89	39·65	40·12
FeO	10·55	12·25	10·01	11·28	12·01	11·67	11·42	11·44	12·08
MnO	0·17	0·12	0·13	0·14	0·28	0·12	0·18	0·18	0·22
MgO	48·06	46·76	48·90	47·78	46·41	46·51	46·69	47·44	46·57
CaO	0·38	0·39	0·40	0·35	0·47	0·47	0·50	0·38	0·44
NiO	0·33	0·20	0·22	0·29	0·23	0·33	0·32	0·25	0·17
Total	99·73	99·18	100·46	99·64	99·91	98·68	98·99	99·33	99·59
Cation fraction (4 oxygens)									
Si	0·996	0·990	0·998	0·989	1·006	0·996	0·998	0·990	1·000
Fe^{2+}	0·218	0·256	0·204	0·235	0·249	0·245	0·239	0·238	0·251
Mn	0·003	0·003	0·003	0·003	0·006	0·003	0·005	0·003	0·004
Mg	1·771	1·747	1·783	1·770	1·717	1·743	1·741	1·765	1·729
Ca	0·010	0·011	0·010	0·009	0·012	0·012	0·014	0·010	0·012
Cation total	2·998	3·007	2·998	3·006	2·990	2·999	2·997	3·006	2·996
Olivine composition									
Fo%	89·04	87·22	89·73	88·28	87·33	87·68	87·93	88·12	87·32

Sample:	nal607	nal609	nal609	nal610	nal610	nal611	nal611	nal600	nal600
Location:	Kistufell	Kistufell	Kistufell	Kistufell	Kistufell	Kistufell	Kistufell	Ridge	Ridge
Size (mm):	0·03	0·20	0·30	0·70	0·20	0·04	0·50	1·00	0·90
ID:	ol5/c	ol1/r	ol4/c	ol2/c	ol4/c	ol2/c	ol4/c	ol1/c	ol5/r
wt %									
SiO_2	39·95	40·44	40·42	39·88	40·27	39·98	40·92	40·92	40·20
FeO	11·47	11·23	11·79	11·16	11·48	12·35	10·92	10·07	11·42
MnO	0·09	0·19	0·11	0·24	0·06	0·19	0·33	0·12	0·16
MgO	46·63	47·61	47·90	47·99	47·35	46·30	47·67	48·45	46·43
CaO	0·49	0·40	0·34	0·36	0·36	0·44	0·36	0·37	0·40
NiO	0·30	0·26	0·28	0·36	0·34	0·16	0·26	0·32	0·24
Total	98·93	100·12	100·83	99·98	99·86	99·41	100·46	100·25	98·85
Cation fraction (4 oxygens)									
Si	1·000	0·999	0·994	0·989	0·998	0·999	1·005	1·003	1·006
Fe^{2+}	0·241	0·231	0·242	0·231	0·238	0·258	0·224	0·206	0·239
Mn	0·002	0·004	0·003	0·004	0·001	0·005	0·007	0·003	0·003
Mg	1·739	1·752	1·754	1·771	1·749	1·725	1·745	1·770	1·732
Ca	0·014	0·010	0·009	0·009	0·009	0·012	0·009	0·010	0·011
Cation total	2·996	2·996	3·002	3·004	2·995	2·999	2·990	2·992	2·991
Olivine composition									
Fo%	87·83	88·35	87·88	88·46	88·02	86·99	88·62	89·57	87·87

Primitive and most evolved olivine compositions in selected samples. c, core; r, rim. Cations on four oxygen basis. All mineral analyses were performed on macrophenocrysts or microphenocrysts *in situ* in handpicked glass shards.

Table 2: Representative electron microprobe analyses of plagioclase

Sample no.:	nal594	nal594	nal595	nal598	nal606	nal606	nal607
Location:	Kistufell	Kistufell	Kistufell	Kistufell	Kistufell	Kistufell	Kistufell
Size (mm):	0·05	0·04	0·02	0·03	0·03	0·02	0·07
ID:	plg2/r	plg4/c	plg1/c	plg3/c	plg1/c	plg2/c	plg3/c
wt %							
SiO_2	47·68	47·24	47·85	47·38	48·99	47·55	48·02
Al_2O_3	34·00	32·71	32·04	31·64	31·01	33·07	31·73
FeO	0·66	0·70	0·83	1·35	1·08	0·66	0·77
CaO	16·16	15·70	16·16	16·71	15·67	16·25	15·85
Na_2O	2·32	2·40	1·98	1·96	2·53	2·12	2·78
K_2O	n.d.	0·04	0·02	0·05	n.d.	0·01	0·05
Total	100·82	98·79	98·88	99·07	99·29	99·66	99·20
Cation fraction (8 oxygens)							
Si	2·173	2·197	2·222	2·208	2·266	2·191	2·227
Al	1·826	1·792	1·754	1·738	1·691	1·796	1·735
Fe	0·025	0·027	0·032	0·053	0·042	0·026	0·030
Ca	0·789	0·782	0·804	0·834	0·777	0·802	0·787
Na	0·205	0·217	0·178	0·177	0·227	0·190	0·250
K	0·000	0·003	0·001	0·003	0·000	0·001	0·003
Cation total	5·017	5·017	4·991	5·013	5·002	5·006	5·032
Plagioclase composition							
An%	79·36	78·11	81·79	82·27	77·40	80·81	75·69
Or%	0·00	0·25	0·10	0·30	0·00	0·08	0·26

a Perkin Elmer Elan 6000 at the University of Durham, UK: 0·1 g of glass shards were digested with HF–HNO_3 in precleaned Teflon vials, and run in dilute (5%) HNO_3 matrix (dilution factor of 500), after spiking with Rh, Re and Bi internal standards. Data reductions include corrections for machine drift, reagent blanks, oxide interferences and isotopic overlaps. The data are calibrated relative to accepted values of a suite of international standard rocks. As the precision is better for this subset of samples (<1% for all elements except Cs <10% based on replicate analyses), the text refers to only these data when incompatible trace elements are being discussed.

Isotope (Sr–Nd–Pb–O–He) analyses were carried out on glasses 408706–408712 only (Table 6). The reproducibility of the NBS 981 standard during the project period was 0·1–0·2% (2 SD) and the measured values average $^{206}Pb/^{204}Pb$ 16·894 ± 0·019, $^{207}Pb/^{204}Pb$ 15·437 ± 0·021 and $^{208}Pb/^{204}Pb$ 36·529 ± 0·071. The errors on the reported He isotope ratios are ±0·17 R/R_a (2 SD). Additional analytical details for He and Pb isotopic analysis have been given by Breddam *et al.* (2000). The Sr and Nd isotopic ratios were measured on a VG-54 sector mass spectrometer at the Danish Centre for Isotope Geology. All handpicked glass fractions (300 mg) were ultrasonically washed (3 × 5 min) in 3 ml 2·5N HCl, followed by rinsing in MQ-water and dissolved directly, without crushing, in 6 ml 8·8N HBr for 3 days. Sr and Nd were extracted after washing through Pb anion exchange columns. The samples were loaded on 20 ml ion exchange columns, washed through with 2·5N HCl, and Sr fractions were subsequently washed through miniature Teflon columns with 3N HNO_3. Nd fractions were cleaned for Ba on miniature Teflon columns (washed with 2N and 4N HNO_3), and subsequently placed on 20 ml ion exchange columns and washed through with 0·25N HCl at 20–21°C. Sr and Nd were loaded with phosphoric acid and HCl, respectively, on Ta centre or side filaments. Sr and Nd isotopic compositions were measured in dynamic mode. During the period of the project and in the months before this the NBS987 Sr standard gave 0·710249 ± 0·000033 (2 SD, n = 45), and the La Jolla (JM Nd standard) gave 0·511106 ±

Sample no.:	nal607	nal609	nal610	nal610	nal611	nal611	nal600
Location:	Kistufell	Kistufell	Kistufell	Kistufell	Kistufell	Kistufell	Ridge
Size (mm):	0·10	0·03	0·07	0·15	0·12	0·09	0·02
ID:	plg1/r	plg1/c	plg1/r	plg2/c	plg1/c	plg4/r	plg1/c
wt %							
SiO_2	45·74	44·66	48·05	45·54	47·42	48·71	47·53
Al_2O_3	34·19	33·96	31·02	34·88	31·50	31·46	32·52
FeO	0·52	0·57	0·80	0·51	0·79	0·67	0·73
CaO	17·75	17·68	15·82	17·84	16·49	15·98	16·56
Na_2O	1·37	1·39	2·73	1·27	1·97	2·55	2·03
K_2O	n.d.	n.d.	0·04	n.d.	0·01	0·01	0·01
Total	99·57	98·25	98·46	100·04	98·17	99·36	99·37
Cation fraction (8 oxygens)							
Si	2·119	2·100	2·245	2·100	2·222	2·250	2·200
Al	1·867	1·882	1·708	1·895	1·739	1·713	1·774
Fe	0·020	0·023	0·031	0·020	0·031	0·026	0·028
Ca	0·881	0·891	0·792	0·882	0·828	0·791	0·821
Na	0·123	0·127	0·248	0·114	0·179	0·228	0·182
K	0·000	0·000	0·003	0·000	0·000	0·001	0·001
Cation total	5·010	5·022	5·026	5·010	4·999	5·008	5·005
Plagioclase composition							
An%	87·73	87·57	75·98	88·59	82·22	77·56	81·83
Or%	0·00	0·00	0·24	0·00	0·02	0·07	0·05

Compositions of plagioclase microphenocrysts and phenocrysts. Cations calculated on eight oxygen basis. c, core; r, rim.

0·000022 (2 SD, $n = 39$). Corrections for radiogenic ingrowth are not applied as all samples are effectively zero-age.

Oxygen isotope analyses of glasses were carried out at Royal Holloway University of London using a laser-fluorination technique (Mattey & Macpherson, 1993). Separates of glass were heated with a CO_2 laser in the presence of BrF_5 and the liberated O_2 was converted to CO_2 by reaction with hot graphite after cleanup with KBr. The CO_2 was subsequently analysed on a VG PRISM mass spectrometer. The O isotope ratios are given in the standard δ notation (per mil deviation from Vienna Standard Mean Ocean Water). Oxygen yields were >96·6% for all analyses. The high yields imply that fractionation can be discounted and suggest that the glasses were not subject to hydration or alteration. The analytical precision during the period of the analyses was judged from the reproducibility of the standard (San Carlos mantle olivine) during the period of the analyses ($\delta^{18}O = 4{\cdot}88 \pm 0{\cdot}15‰$, $n = 5$, 2 SD).

RESULTS

Mineral chemistry

Hyaloclastites, pillow rims and basalts from Kistufell and the hyaloclastite ridge (nal600) contain olivine phenocrysts, occasional Cr-spinel or plagioclase phenocrysts (>100 μm), and ubiquitous olivine, Cr-spinel and plagioclase microphenocrysts (<100 μm) scattered in a glassy or cryptocrystalline (not analysed) groundmass. The mineral phases are essentially euhedral and occur individually or in aggregates. Modal compositions, roughly estimated by eye, indicate that phenocrysts are less abundant (<4%) in the eastern flank pillow mounds and the cap-lava relative to pillows and hyaloclastites from the northern flank (4–8%).

Olivine phenocrysts are unfragmented with abundant inclusions of Cr-spinel and often occur in clusters of grains, rarely exceeding 500 μm. They are generally of Mg-rich composition $Fo_{89·7–87·9}$ (cores: Table 1), similar to olivines in primary MORB (Hess, 1992). The rims are

Table 3: Representative electron microprobe analyses of chromian spinel

Sample no.:	nal594	nal594	nal595	nal595	nal606	nal606	nal608	nal608
Location:	Kistufell	Kistufell	Kistufell	Kistufell	Kistufell	Kistufell	Kistufell	Kistufell
Size (mm):	0·095	0·095	0·35	0·12	0·03	0·03	0·03	0·15
ID:	sp7/c	sp7/r	sp1/c	sp2/r	sp2/μ	sp3/μ	sp4/μ	sp5/c
wt %								
TiO_2	0·29	0·31	0·23	0·36	0·43	0·42	0·42	0·43
Al_2O_3	31·97	38·72	36·83	39·89	36·94	34·49	38·75	34·65
Cr_2O_3	32·36	25·38	29·27	24·63	26·19	28·84	24·29	30·41
FeO*	9·48	7·76	9·99	10·99	11·86	11·93	9·77	11·71
Fe_2O*	7·11	7·99	4·87	5·19	6·47	6·71	7·27	5·51
MnO	0·13	0·16	0·10	0·13	0·22	0·17	0·16	0·18
MgO	17·71	19·76	18·06	17·63	16·73	16·48	18·48	16·79
NiO	0·28	0·33	0·15	0·25	0·21	0·23	0·19	0·24
Total	99·33	100·41	99·50	99·07	99·05	99·27	99·86	99·93
Cation fraction (32 oxygens)								
Al	8·733	10·121	9·840	10·603	9·982	9·405	10·236	9·375
Ti	0·056	0·054	0·041	0·068	0·069	0·070	0·068	0·069
Fe^{2+}	1·836	1·438	1·894	2·075	2·275	2·310	1·832	2·247
Fe^{3+}	1·251	1·332	0·818	0·868	1·131	1·169	1·239	0·965
Mn	0·028	0·027	0·014	0·027	0·041	0·028	0·027	0·041
Mg	6·105	6·525	6·106	5·925	5·722	5·690	6·168	5·749
Cr	5·925	4·448	5·261	4·393	4·743	5·287	4·391	5·515
Total	23·990	23·998	24·001	24·000	24·004	24·001	24·001	24·002
Cr-spinel composition								
mg-no.	0·769	0·819	0·763	0·741	0·716	0·711	0·771	0·719
cr-no.	0·404	0·305	0·348	0·293	0·322	0·360	0·300	0·370

usually more Fe enriched ($Fo_{87·8–87·2}$), and compositionally similar to the microphenocrysts ($Fo_{88·1–87·0}$) (Table 1). The nickel contents of the olivines are between 1250 and 2800 ppm and in equilibrium with the matrix glass (Elthon, 1987). As the oxidation state of iron in the melt was independently determined by Mössbauer spectroscopy (Table 4) the degree of olivine–melt equilibrium can be evaluated precisely in terms of *mg*-number [$100Mg^{2+}/(Mg^{2+} + Fe^{2+})$]. Equilibrium olivine compositions calculated from glass compositions (Table 4) correspond to the observed microphenocryst compositions (Table 1) and generally the K_d values ($Fe–Mg^{ol–liq}$) (Roeder & Emslie, 1970) are near 0·30 (Fig. 2a), within the K_d range (0·26–0·34) observed for Icelandic hyaloclastites (Mäkipää, 1978*a*). Assuming that the most primitive phenocryst core ($Fo_{89·7}$) equilibrated at K_d = 0·30, the calculated parental melt had an *mg*-number of 72·5. Some phenocrysts (≪1 vol. %, visually estimated) found in nal595 have abundant melt and gas inclusions, but no spinel inclusions. These phenocrysts are reversely zoned ($Fo_{87–85}$), have a different petrographic appearance (fragmented) and are not in equilibrium with their host glass (Fig. 2a).

Plagioclase microphenocryst compositions ($An_{82·3–75·7}$) (Table 2) vary by <1·5 An% within the individual crystals. Calculated K_d values ($Na–Ca^{plg–liq}$) range from 1·0 to 1·3, similar to K_d values calculated here for other rift zone lavas (Fig. 2b) but are high relative to MORB from the Mid-Atlantic Ridge (MAR) (0·63–1·11, Niu & Batiza, 1994). Phenocrysts (≪1 vol. %, visually estimated) and some microphenocrysts (phenocryst fragments?) in three samples (nal607, nal609 and nal610) have high An contents (85·5–88·6%, Fig. 2b), some examples of which are reported in Table 2. These phenocrysts are sometimes fragmented and contain abundant gas or melt inclusions, and sometimes display irregular or complex zoning (see Discussion).

Chromian spinel occurs as microphenocrysts in the groundmass or as inclusions in olivine, and as phenocrysts (≪1 vol. % visually estimated) within clusters of olivine.

Sample no.:	nal609	nal609	nal610	nal610	nal611	nal611	nal600	nal600
Location:	Kistufell	Kistufell	Kistufell	Kistufell	Kistufell	Kistufell	Ridge	Ridge
Size (mm):	0·03	0·05	0·02	0·02	0·11	0·11	0·05	0·04
ID:	sp3/μ	sp4/μ	sp1/μ	sp2/μ	sp1/c	sp2/r	sp1/μ	sp2/μ
wt %								
TiO_2	0·35	0·33	0·34	0·38	0·42	0·44	0·24	0·35
Al_2O_3	37·13	35·12	37·67	34·92	37·15	35·43	31·07	32·71
Cr_2O_3	24·84	26·90	24·92	26·64	26·29	28·85	33·37	33·42
FeO*	11·21	11·21	10·49	9·63	9·92	11·78	11·14	12·21
Fe_2O*	6·79	6·87	7·59	8·70	7·27	5·75	6·31	5·27
MnO	0·09	0·06	0·33	0·09	0·14	0·10	0·18	0·16
MgO	16·68	16·63	17·51	17·73	18·13	16·69	16·48	16·44
NiO	0·64	0·26	0·40	0·47	0·24	0·31	0·25	0·20
Total	97·73	97·38	99·25	98·56	99·57	99·35	99·04	100·76
Cation fraction (32 oxygens)								
Al	10·137	9·686	10·088	9·500	9·905	9·621	8·595	8·882
Ti	0·056	0·057	0·055	0·070	0·068	0·069	0·043	0·056
Fe^{2+}	2·172	2·196	1·996	1·861	1·878	2·267	2·184	2·352
Fe^{3+}	1·197	1·211	1·312	1·500	1·252	0·995	1·127	0·913
Mn	0·014	0·014	0·068	0·014	0·027	0·014	0·042	0·028
Mg	5·765	5·814	5·933	6·111	6·122	5·723	5·763	5·645
Cr	4·539	4·984	4·483	4·861	4·707	5·253	6·200	6·087
Total	24·005	24·004	24·003	24·000	24·000	23·997	23·996	24·005
Cr-spinel composition								
mg-no.	0·726	0·726	0·748	0·767	0·765	0·716	0·725	0·706
cr-no.	0·309	0·340	0·308	0·339	0·322	0·353	0·419	0·407

*Recalculated from total iron (FeO^t) as FeO, based on stoichiometry.
μ, microphenocryst; c, core; r, rim.

Occasionally, the phenocrysts display dark rims. The compositional range is *cr*-number = 0·26–0·42 and *mg*-number = 0·69–0·82 (Table 3 and Fig. 3a and b) with minor TiO_2 (0·23–0·55%), NiO (0·06–0·64%) and MnO (0·06–0·33%). Phenocrysts have Cr-rich unzoned cores, with *mg*-number fluctuating around a mean value, and rims strongly zoned towards lower *cr*-number and sometimes higher *mg*-number (Fig. 4a). The rim zonation is occasionally reversed towards higher *cr*-number and lower *mg*-number. Unzoned and reversely zoned phenocrysts also occur and can be found within the same sample. Groundmass microphenocrysts and inclusions have similar unzoned compositions (*cr*-number 0·30–0·32), matching the phenocryst rims (Table 2). Relatively high *cr*-numbers characterize Cr-spinel in the hyaloclastite ridge sample (nal600) compared with Kistufell (Fig. 3b).

Whole-rock and glass chemistry

Major and trace element compositions of basalts and fresh glass handpicked from pillow rims or hyaloclastites are presented in Tables 4 and 5, together with Mössbauer Fe^{3+}/Fe^{tot} analyses on selected glass separates (nal595, nal600, nal611). The glasses (MgO 9·27–10·56 wt %) are among the most MgO rich found in Iceland (Mäkipää, 1978*b*; Sigurdsson, 1981; Meyer *et al.*, 1985; Werner, 1994; Gurenko & Chaussidon, 1995; Schiellerup, 1995; Hansen & Grönvold, 2000; Slater *et al.*, 2001). The Mössbauer measurements, which allow accurate calculation of *mg*-number values, reveal some of the most reduced Fe^{2+}/Fe^{tot} ratios (>0·92) observed in Iceland. Expressed in log fO_2 units the glass separates range from −10·25 to −10·82, which is essentially identical to the range of values (log fO_2 −10·36 to −10·78) calculated

Table 4: Representative electron microprobe analyses of basaltic glasses

Sample no.:	nal594	nal595	nal596	nal598	nal606	nal607	nal609	nal610	nal611	nal600
Location:	Kistufell	Kistufell	Kistufell	Kistufell	Kistufell	Kistufell	Kistufell	Kistufell	Kistufell	Ridge
Rock type:	hya	rim	hya	hya	hya	hya	hya	hya	rim	rim
No. of grains:	5	3	4	3	5	4	3	3	5	5
No. of analyses:	10	6	7	6	9	8	6	6	10	10
wt %										
SiO_2	48·45	48·32	48·34	48·43	48·42	48·15	47·70	47·90	48·67	48·98
TiO_2	0·94	0·93	0·92	0·92	1·08	1·05	1·04	1·00	1·11	0·87
Al_2O_3	16·25	15·99	16·28	15·94	15·89	15·75	16·12	16·08	15·34	15·10
FeO^t	9·18	8·96	9·01	9·03	9·49	9·28	9·28	9·39	9·49	8·69
MnO	0·15	0·16	0·16	0·15	0·16	0·18	0·17	0·17	0·17	0·16
MgO	9·35	10·56	9·51	9·60	9·27	9·35	9·67	9·55	10·02	10·18
CaO	13·93	14·01	13·77	14·09	13·85	13·49	13·75	13·56	13·51	14·04
Na_2O	1·72	1·72	1·78	1·84	1·87	1·84	1·81	1·73	1·75	1·71
K_2O	0·07	0·05	0·08	0·08	0·09	0·08	0·06	0·06	0·07	0·06
P_2O_5	0·05	n.d.	0·08	0·04	0·18	0·05	0·01	0·03	0·07	0·05
Total	100·10	100·68	99·93	100·12	100·29	99·21	99·62	99·46	100·19	99·84
Original compositional parameters										
mg-no.	66·86	70·01	67·65	67·80	65·93	66·62	67·36	66·83	67·65	69·88
Fo% (eq-ol)	87·44	88·96	87·83	87·90	86·97	87·32	87·69	87·42	87·83	88·90
Mössbauer analyses and corrections										
$(Fe^{3+}/Fe^{tot}) \times 100$		6·65*							6·77*	5·22*
FeO	8·56	8·36	8·41	8·42	8·85	8·66	8·66	8·76	8·85	8·24
Fe_2O_3	0·68	0·67	0·67	0·67	0·71	0·69	0·69	0·70	·071	0·50
Log fO_2 (Mössbauer)	−10·25							−10·25	−10·82	
Log fO_2 (Cr-spinel)		−10·53							−10·36	−10·78
Derived compositional parameters										
mg-no.	66·06	69·24	66·86	67·02	65·12	65·82	66·57	66·03	66·88	68·78
Fo% (eq-ol)	86·65	88·24	87·05	87·13	86·15	86·52	86·91	86·63	87·06	88·02

Compositions are averages of 6–10 analyses in 3–5 handpicked grains. FeO^t, total iron as FeO. *mg*-number = 100 × Mg/(Mg + Fe^{2+}) with $Fe^{2+}/(Fe^{2+} + Fe^{3+})$ = 0·90. Equilibrium olivine compositions calculated from glass compositions (K_d = 0·3). Log fO_2 values were also calculated from Cr-spinel compositions following the equation given by Roeder (1982) for systems at 1200°C. It should be noted that log fO_2 values for Mössbauer analyses closely agree with those calculated from the observed Cr-spinel compositions.
*Oxidation state of iron (glass) measured by Mössbauer spectroscopy at Science Institute, University of Iceland.

from Cr-spinel compositions in the same samples (following Roeder, 1982). Whole rocks have *mg*-number (67·4–72·6), Al_2O_3 (14·6–16·5 wt %), FeO^{tot} (8·65–9·98 wt %) TiO_2 (0·87–1·06 wt %) and K_2O (0·04–0·09 wt %) comparable with primitive olivine tholeiites from Iceland and North Atlantic N-MORB (Fig. 5). However, concentrations of SiO_2 (47·8–49·6 wt %) and Na_2O (1·24–1·89 wt %) in Kistufell, and Icelandic basalts in general, are low relative to average North Atlantic N-MORB. CaO abundances also deviate from average N-MORB, being generally higher in Icelandic basalts, including Kistufell (11·0–13·3 wt %) (Fig. 5). The effects of fractional crystallization at pressures equivalent to those prevailing in the upper and lower Icelandic crust were evaluated using COMAGMAT (Ariskin *et al.*, 1993). The models show that low-pressure fractionation (2 kbar:

Table 5: Major (ICP-AES and XRF) and trace (ICP-MS) element analyses

Sample:	nal594	nal594	nal595	nal595	nal596	nal598	nal606	nal607	nal608	nal609
Locality:	Kistufell	Kistufell	Kistufell	Kistufell	Kistufell	Kistufell	Kistufell	Kistufell	Kistufell	Kistufell
Rock type:	pill.rim	hya	pill.bas	pill.rim	hya	hya	hya	hya	cap-lava	hya
wt %										
SiO_2	48·76	49·02	49·15	49·58	48·86	49·07	47·78	48·20	48·38	48·55
TiO_2	0·89	0·87	0·90	0·92	0·91	0·98	1·02	0·99	1·03	1·04
Al_2O_3	16·08	15·73	15·61	15·55	16·01	15·86	15·20	15·32	15·99	16·51
FeO^t	8·95	9·01	9·19	8·88	9·04	9·35	9·67	9·69	9·41	9·92
MnO	0·15	0·15	0·15	0·15	0·16	0·16	0·16	0·16	0·16	0·17
CaO	13·33	12·84	12·82	12·59	12·69	12·40	11·89	12·06	12·84	11·00
MgO	9·89	10·44	10·14	10·31	10·28	10·17	12·16	11·61	10·08	10·95
Na_2O	1·67	1·68	1·78	1·80	1·77	1·74	1·79	1·67	1·84	1·56
K_2O	0·07	0·06	0·07	0·08	0·06	0·08	0·08	0·08	0·07	0·08
P_2O_5	0·08	0·08	0·08	0·05	0·09	0·08	0·09	0·08	0·08	0·07
Total	99·88	99·88	99·90	99·91	99·87	99·89	99·84	99·86	99·88	99·84
mg-no.	68·03	69·05	67·99	69·09	68·65	67·68	70·77	69·76	67·35	68·00
ppm										
Sc	38·0	38·0	38·4	38·6	39·9	38·0	37·9	36·8	38·9	40·2
V	231	227	237	233	245	235	223	229	258	219
Cr	286	313	291	297	323	341	588	536	330	575
Co	46·1	48·7	48·0	48·0	51·0	49·0	54·1	53·2	51·0	54·5
Ni	195	231	208	218	234	221	315	287	216	290
Cu	108	111	110	112	114	121	111	113	116	115
Zn	64·6	64·9	64·9	68·5	69·2	71·7	76·7	70·4	71·6	73·3
Y	16·2	16·2	16·2	16·1	17·0	17·5	17·5	17·0	18·0	17·2
Zr	38·7	38·7	41·4	42·9	42·8	43·5	50·9	45·0	46·8	46·5
Hf	—	—	—	—	—	—	—	—	—	—
Nb	2·32	2·49	2·70	2·87	2·83	2·83	3·19	2·86	2·90	2·85
Mo	0·17	0·07	0·20	0·18	0·19	0·12	0·20	0·16	0·10	0·10
Ta	0·18	0·20	0·21	0·22	0·22	0·21	0·25	0·22	0·22	0·22
Rb	0·96	1·09	1·20	1·20	1·09	1·20	1·21	1·19	1·21	1·41
Sr	116	120	121	119	126	124	123	123	137	127
Cs	0·018	0·002	0·011	0·012	0·035	0·029	0·048	0·046	0·050	0·052
Ba	12	13	15	15	18	15	16	15	15	15
Th	0·11	0·13	0·14	0·14	0·14	0·15	0·14	0·14	0·13	0·13
U	0·012	0·029	0·039	0·028	0·041	0·037	0·031	0·030	0·012	0·027
Pb	—	0·07	—	—	—	0·01	—	—	—	—
La	2·19	2·29	2·60	2·58	2·60	2·47	2·76	2·44	2·67	2·67
Ce	5·81	5·77	6·53	6·93	6·69	6·91	7·61	6·86	7·16	6·97
Pr	0·95	0·88	0·97	0·98	0·99	1·04	1·12	1·00	1·04	0·98
Nd	4·52	4·95	4·83	4·99	5·34	4·85	5·91	5·87	5·65	5·97
Sm	1·78	1·80	1·85	1·71	1·71	1·87	1·75	1·74	2·03	1·90
Eu	0·73	0·66	0·70	0·72	0·72	0·77	0·77	0·71	0·74	0·74
Gd	2·49	2·42	2·35	2·25	2·43	2·47	2·62	2·65	2·47	2·67
Tb	0·39	0·36	0·40	0·40	0·40	0·42	0·45	0·43	0·44	0·45
Dy	2·50	2·60	2·77	2·66	2·91	2·81	2·89	2·76	2·90	2·81
Ho	0·58	0·58	0·68	0·61	0·64	0·61	0·71	0·65	0·72	0·66
Er	1·57	1·59	1·51	1·55	1·56	1·61	1·71	1·53	1·71	1·56
Tm	0·25	0·25	0·26	0·23	0·23	0·24	0·28	0·27	0·27	0·25
Yb	1·56	1·69	1·69	1·66	1·48	1·55	1·79	1·73	1·85	1·68
Lu	0·22	0·27	0·22	0·23	0·30	0·29	0·26	0·23	0·32	0·31

Table 5: continued

Sample:	nal610	nal611	nal611	nal600	nal600	408706	408707	408709	408710	408712	BTHO
Locality:	Kistufell	Kistufell	Kistufell	Ridge	Ridge	Kistufell	Kistufell	Kistufell	Kistufell	Kistufell	
Rock type:	hya	pill.bas	pill.rim	pill.bas	pill.rim	pill.rim	pill.rim	pill.rim	pill.rim	pill.rim	basalt
wt %											
SiO_2	48·05	47·91	48·54	49·15	49·23	48·13	47·87	48·26	47·99	47·92	
TiO_2	1·06	1·06	1·01	0·84	0·85	0·90	0·90	0·90	0·88	1·02	
Al_2O_3	16·30	16·01	15·05	14·77	14·59	16·32	16·12	16·33	16·16	15·99	
FeO^t	9·98	9·54	9·24	8·65	8·94	8·85	8·76	8·95	8·91	9·11	
MnO	0·16	0·16	0·16	0·15	0·16	0·15	0·16	0·16	0·16	0·16	
CaO	11·54	12·69	12·24	13·31	12·59	12·86	12·74	12·86	12·74	12·53	
MgO	11·06	10·45	11·68	11·27	11·60	10·34	10·43	10·29	10·43	10·51	
Na_2O	1·53	1·89	1·80	1·54	1·75	1·74	1·73	1·75	1·72	1·79	
K_2O	0·08	0·08	0·08	0·07	0·06	0·08	0·07	0·07	0·07	0·08	
P_2O_5	0·09	0·09	0·07	0·08	0·08	0·07	0·07	0·08	0·07	0·07	
Total	99·85	99·88	99·87	99·83	99·85	99·96	99·24	99·89	99·49	99·53	
mg-no.	68·09	67·84	70·88	71·15	71·06	69·69	69·87	69·19	70·02	69·62	
ppm											
Sc	40·4	37·4	36·7	41·6	39·7	—	—	—	—	—	—
V	227	257	238	253	241	—	—	—	—	—	311
Cr	548	384	479	747	586	—	—	—	—	—	555*
Co	53·3	49·6	52·5	51·8	52·6	—	—	—	—	—	49·9
Ni	285	223	292	295	285	—	—	—	—	—	198
Cu	115	111	114	105	123	—	—	—	—	—	112
Zn	73·0	70·8	69·3	65·8	68·1	—	—	—	—	—	69·6
Y	17·4	18·1	17·2	16·7	16·5	17·8	18·7	18·1	18·1	19·2	15·1
Zr	46·4	47·8	44·5	44·3	46·1	38·9	42·6	41·1	41·3	45·1	15·3
Hf	—	—	—	—	—	1·13	1·24	1·22	1·83	1·28	—
Nb	2·90	3·00	2·79	2·44	2·54	2·98	3·36	3·50	3·35	3·56	0·48
Mo	0·08	0·13	0·19	0·14	0·15	—	—	—	—	—	0·03
Ta	0·23	0·22	0·21	0·18	0·18	0·197	0·236	0·247	0·227	0·237	0·05
Rb	1·21	1·37	1·44	1·02	1·32	1·059	1·149	1·109	1·119	1·072	0·35
Sr	121	134	124	111	108	120	127	121	121	130	112
Cs	0·038	0·049	0·039	0·023	0·066	0·010	0·009	0·008	0·016	0·010	0·037
Ba	15	14	15	13	13	14·1	15·4	14·7	14·9	15·6	5·8
Th	0·13	0·13	0·12	0·12	0·13	0·161	0·181	0·172	0·168	0·164	0·008
U	0·023	0·018	0·033	0·023	0·047	0·046	0·054	0·051	0·052	0·048	—
Pb	—	—	—	—	—	0·209	0·299	0·234	0·221	0·215	0·3
La	2·59	2·69	2·64	2·33	2·52	2·20	2·50	2·43	2·41	2·50	0·63
Ce	7·26	7·26	6·88	6·29	6·79	5·87	6·59	6·50	6·38	6·77	1·82
Pr	1·05	1·08	1·03	0·97	0·96	0·93	1·03	1·03	1·01	1·09	0·36
Nd	5·72	5·82	5·18	4·93	5·78	5·03	5·51	5·39	5·43	5·86	2·23
Sm	1·97	2·01	1·71	1·91	1·70	1·71	1·83	1·82	1·79	1·96	1·00
Eu	0·72	0·81	0·79	0·77	0·71	0·67	0·72	0·70	0·96	0·77	0·49
Gd	2·61	2·60	2·55	2·35	2·59	2·39	2·56	2·48	2·45	2·72	1·92
Tb	0·42	0·45	0·40	0·40	0·42	0·43	0·46	0·46	0·44	0·48	0·33
Dy	2·97	3·06	2·66	2·82	2·65	2·84	2·97	2·94	2·87	3·05	2·13
Ho	0·67	0·71	0·62	0·63	0·67	0·61	0·65	0·64	0·62	0·66	0·54
Er	1·66	1·75	1·77	1·72	1·55	1·686	1·844	1·816	1·753	1·888	1·48
Tm	0·26	0·29	0·25	0·22	0·26	0·263	0·284	0·278	0·273	0·288	0·24
Yb	1·85	1·86	1·67	1·56	1·72	1·68	1·82	1·75	1·71	1·86	1·65
Lu	0·30	0·32	0·29	0·27	0·29	0·263	0·279	0·269	0·264	0·286	0·27

mg-number = 100 × Mg/(Mg + Fe^{2+}) with $Fe^{2+}/(Fe^{2+} + Fe^{3+})$ calculated from Mössbauer data (Table 4). pill. bas, pillow basalt interior; pill. rim, outer glass rim; hya, hyaloclastite; cap-lava, upper subaerially erupted lava; —, not measured.
*Cr values were determined by ICP-AES (NVI), except for BTHO (see analytical techniques section).

Table 6: Sr, Nd, O, (Pb, He) isotope ratios of basaltic glasses*

Sample no.:	$^{87}Sr/^{86}Sr$	$^{143}Nd/^{144}Nd$	$\delta^{18}O$	$^{3}He/^{4}He$	$^{206}Pb/^{204}Pb$	$^{207}Pb/^{204}Pb$	$^{208}Pb/^{204}Pb$
408706	0·703036	0·513073	4·74	15·33	18·343	15·431	37·953
408707	0·703060	—	—	15·69	18·346	15·420	37·935
408709	—	0·513099	4·60	15·65	18·361	15·431	37·964
408710	0·703060	0·513076	4·46	15·79	18·355	15·427	37·954
408712	0·703079	0·513058	4·43	16·79	—	—	—

*Previously published in Breddam *et al.* (2000), where also analytical data can be found.

Fig. 5) can explain the broad major element variations within Iceland lavas, although some compositions seem to require fractionation at higher pressures (8 kbar: Fig. 5). Inflections in the data arrays suggest fractionation of olivine followed by ol + plg, ol + plg + cpx, ol + plg + cpx + mgt at low pressure (2 kbar) or opx + cpx + plg, opx + cpx + plg + mgt at higher pressure (8 kbar) (Fig. 5). The observed compositional difference between whole rocks (glass + crystals) and glasses can be accounted for by subtraction of 4 vol. % olivine ($Fo_{88·6–87·2}$) on average (Fig. 5).

The trace element abundances normalized to primitive mantle show almost identical, slightly light rare earth element (LREE) depleted (La_n/Yb_n = 0·89–0·96, Ba_n/Zr_n = 0·55–0·58), convex-upward patterns (La_n/Sm_n = 0·80–0·86, Sm_n/Yb_n = 1·09–1·15) (ICP-MS data; Fig. 6a). Several anomalies (positive Nb, Ta and Sr, and negative Pb and K) disturb the otherwise smooth patterns and, for example, produce low K/Nb, La/Nb and Zr/Nb. Similar anomalies are also present in picrites, tholeiites and alkaline basalts (except Sr) in Iceland (Elliott *et al.*, 1991; Furman *et al.*, 1991; Hemond *et al.*, 1993; Hards *et al.*, 1995; Chauvel & Hemond, 2000) and will be discussed below. It is evident from Fig. 6b that the hyaloclastite ridge (nal600) is compositionally identical to Kistufell, in terms of incompatible trace elements. In general, Kistufell is as incompatible element depleted as the most depleted ol-tholeiites in Iceland, both in terms of concentrations and with respect to depletion of highly incompatible trace elements relative to less incompatible elements. Only Icelandic picrites are more depleted in incompatible elements. This feature is also observable from the Nb/Y vs Zr/Y diagram, in which Kistufell clearly plots within the most depleted part of the Iceland array as defined by Fitton *et al.* (1997) (Fig. 7).

Sr, Nd, Pb, He and O isotopic compositions of the handpicked glasses show a very limited range of variation relative to that displayed by Iceland as a whole (Table 6). In fact, the Sr, Nd, Pb and O isotopic ranges are within error, which suggests that the samples belong to the same eruptive unit. It should, however, be noted that sample 408712 from the base of the table mountain has the lowest $^{143}Nd/^{144}Nd$ and $\delta^{18}O$, and the highest $^{87}Sr/^{86}Sr$ and $^{3}He/^{4}He$ ratios observed at Kistufell. This may indicate that there is a subtle geochemical gradient from the first to the last erupted portions of the structure. Furthermore, the same sample (408712) defines the upper or lower bound of the range of variation of most major and trace elements (Al_2O_3, CaO, MgO, FeO^{tot}, TiO_2, K_2O, Ba, Sr, Nb, Zr, Y, REE except Eu). In general, Kistufell has 'depleted' signatures with isotopic ratios ($^{87}Sr/^{86}Sr$ 0·703036–0·703079, $^{143}Nd/^{144}Nd$ 0·513058–0·513099, $^{206}Pb/^{204}Pb$ 18·343–18·361, $^{207}Pb/^{204}Pb$ 15·420–15·431, $^{208}Pb/^{204}Pb$ 37·935–37·954) like most Icelandic olivine tholeiites (e.g. Chauvel & Hemond, 2000). In particular, the Pb isotopic ratios are among the most unradiogenic in Iceland (Fig. 8a and b) and only MORB-influenced tholeiites and some picrites show more 'depleted' ratios (Elliott *et al.* 1991; Hardarson *et al.*, 1997; Hanan *et al.*, 2000).

To relate Kistufell to different suggested mantle source components, all the published data for Icelandic basalts are plotted in diagrams of $^{87}Sr/^{86}Sr$ vs $^{206}Pb/^{204}Pb$ and $^{143}Nd/^{144}Nd$ vs $^{206}Pb/^{204}Pb$ along with North Atlantic MORB, Northern Hemisphere ocean-island basalts (OIB), St. Helena HIMU (high $^{238}U/^{204}Pb$) and the Focal Zone (FOZO) component for reference (Fig. 8c and d). North Atlantic MORB and Icelandic basalts form subparallel arrays between a depleted MORB mantle (DMM) component and a HIMU component, with the Iceland array displaced slightly in the direction of enriched mantle components EM1 and EM2. The $^{3}He/^{4}He$ ratios (15·3–16·8 R/R_a) are elevated relative to N-MORB (9·13 $\pm$ 3·57 R/R_a); a feature that is common to basalts in Iceland and frequently regarded as an indicator of the involvement of an undegassed mantle source component (e.g. Kurz *et al.*, 1982, 1985; Breddam *et al.*, 2000), which could be FOZO (Hilton *et al.*, 1999).

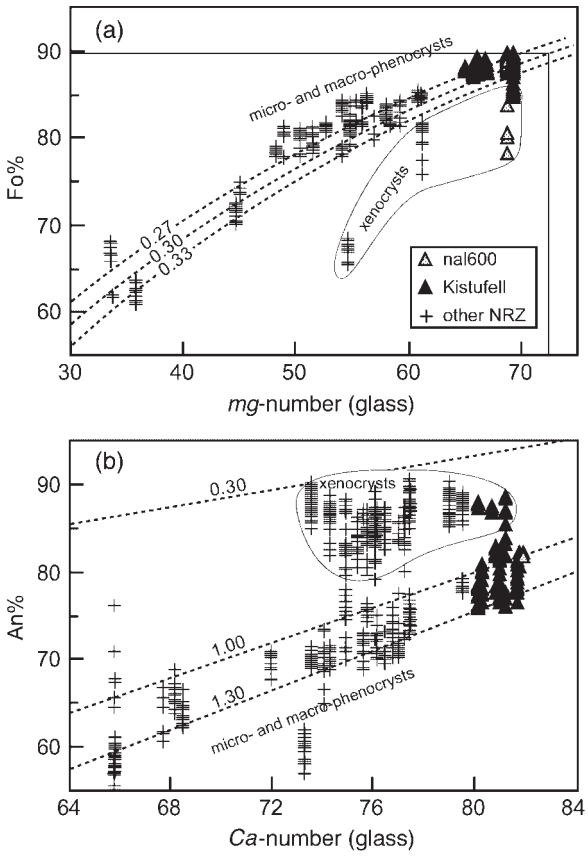

Fig. 2. (a) Olivine (Fo%) vs host glass *mg*-number [Mg/(Mg + Fe^{2+})] and Fe^{2+} from Mössbauer analysis (Table 4). Both core and rim data are shown. Olivine–glass pairs from Kistufell and the related ridge (nal600) are shown in relation to the range of Northern Rift Zone samples (K. Breddam, unpublished data, 1996). Equilibrium olivine compositions are shown for K_d values of 0·27, 0·30 and 0·33 (dashed lines). The olivine rims (Kistufell and nal600) are generally in Mg–Fe exchange equilibrium with the glass at a K_d value of 0·30. They are therefore thought to have formed from the melt, probably during magma transport through the crust immediately before the eruption. The olivine cores are not in equilibrium with the glass and are believed to have formed at an earlier stage, when the magma was even more Mg rich. The *mg*-number of the melt corresponding to the most primitive ol-phenocryst (core) is shown graphically (72·5). (b) Plagioclase (An%) vs host glass *ca*-number [Ca/(Ca + Na)]. Macro- and microphenocryst compositions equilibrated at $K_d(Na–Ca)^{plg–liq}$ between 1·00 and 1·30. Some plagioclase macrocrysts are interpreted as xenocrysts on the basis of their position well outside reasonable K_d values. It should be noted that only a few xenocrysts were observed in Kistufell.

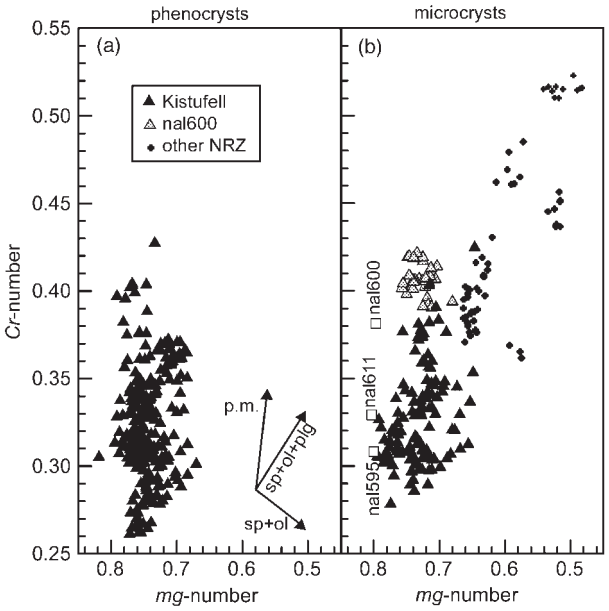

Fig. 3. Cr-spinel compositions: *cr*-number [Cr/(Cr + Al)] vs *mg*-number [Mg/(Mg + Fe^{2+})] for Kistufell, nal600 (related ridge) and NRZ samples for reference (K. Breddam, unpublished data, 1996). Symbols as in Fig. 2. (a) Phenocrysts; (b) microphenocrysts. □, equilibrium Cr-spinel compositions calculated from bulk composition of nal595, nal600, nal611 (Table 5) at 10 kbar (SPINMELT, Ariskin & Nikolaev, 1996). It should be noted that 10 kbar compositions correspond to the majority of microphenocrysts encountered in the samples. Also, in nal600, which has no spinel phenocrysts, the compositions of the microphenocrysts are the same as that of phenocryst cores in Kistufell (nal594: Fig. 4). Qualitative effects of partial melting (p.m.) and fractionation of sp + ol and sp + ol + plg are outlined.

However, Kistufell displays $^{87}Sr/^{86}Sr$, $^{207}Pb/^{204}Pb$ and $^{208}Pb/^{204}Pb$ ratios that are somewhat depleted relative to the FOZO component. Finally, Kistufell lavas have uniform $\delta^{18}O$ values (+4·4‰ to +4·7‰) that vary within the analytical uncertainty. Like the majority of Icelandic lavas (e.g. Hemond *et al.*, 1993; Gee *et al.*, 1998*b*), the $\delta^{18}O$ values are low relative to estimated Iceland mantle values (5·2 ± 0·2‰ Gautason & Muehlenbachs, 1998). Low $\delta^{18}O$ values in Icelandic lavas are frequently ascribed to interaction with hydrothermally altered crust (Gautason & Muehlenbachs, 1998), but have also been attributed to an intrinsic plume component (Thirlwall *et al.*, 1999).

DISCUSSION

Primary magmas at Kistufell

Estimate of primary magma composition

Primary basalts should: (1) have olivine as the only liquidus phase at one atmosphere; (2) coexist with all residual phases in the mantle; (3) be in Fe–Mg exchange equilibrium with mantle olivine (*mg*-$number_{melt}$ >68); (4) crystallize olivine with Fo% 88–91 (Fo% ~90 where melting approaches the diopside-out curve); (5) have Ni contents (300–400 ppm) in equilibrium with mantle olivine (Hess, 1992). The most primitive Kistufell rocks (nal595, nal600, nal606, nal611, 408706–408712) meet these requirements. However, the Ni contents suggest that a small percentage of olivine has fractionated (Fig. 9). As the bulk-rock (glass + crystals) Ni values are in equilibrium with the olivine phenocryst cores, the

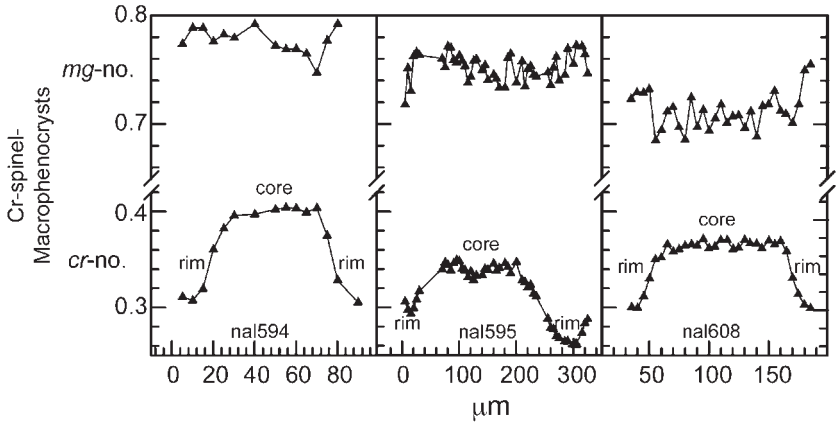

Fig. 4. *cr*-number and *mg*-number traverses across Cr-spinel macrocrysts. Symbols as in Fig. 3. The zonation towards more Al-rich rims is believed to reflect that the macrophenocrysts were relatively Cr rich when they were incorporated into Kistufell magma, which at the time was plagioclase undersaturated and thus crystallized more Al-rich (Cr-poor) Cr-spinels. The late-stage onset of plagioclase crystallization (in addition to sp + ol) is believed to explain the zoning reversal in nal595.

bulk-rock compositions can be regarded as melt equivalents and the amount of fractionated olivine ($1 - F$) can be estimated. The MgO and Ni contents of the assumed primary magma can be determined from the intersection of the series of theoretical liquids in equilibrium with mantle olivine ($Fo_{90–92}$ and 2850 ppm Ni: Bernstein *et al.*, 1998) and the continuation of the fractionation trend (regression) (Fig. 9). If $F = C_L/C_O^{1/(D-1)}$, where C_L/C_O is the ratio of Ni concentrations in the fractionated liquid (nal606) and the graphically estimated primary magma, and $D^{Ni} = 122{\cdot}16/MgO - 2{\cdot}27$ (Elthon, 1987), then $1 - F$ amounts to <4 wt %. A 'primary' composition is calculated by adding 4% olivine to nal606, by recalculating liquid composition and new equilibrium olivine in increments of 1 wt %. This sample was chosen because it is the most primitive sample and therefore illustrates the minimum amount of fractionation. The calculated 'primary' liquid agrees with that estimated graphically (Fig. 2a) and has 13·6 wt % MgO, 47·5 wt % SiO_2, and *mg*-number 72·8. It resembles the aggregated melts of Kinzler & Grove (1992*a*, 1992*b*), which were generated over a range of pressures (4–25 kbar: MgO 12·4 wt %, SiO_2 47·8 wt %, *mg*-number 72·8) and calculated using constraints provided by experiments on multiply saturated liquids. Such MgO-rich basalts can be interpreted as either primary or near-primary magmas generated at ~10 kbar (Hart & Davies, 1978; Presnall & Hoover, 1978; Takahashi & Kushiro, 1983; Fujii & Scarfe, 1985; Fujii, 1989) or as derivatives of picrites (16–18 wt % MgO) produced at high pressures (20–30 kbar) (O'Hara, 1968; Elthon, 1989). The fundamental argument against the former view, that low SiO_2 (<49·7 wt %) in most MgO-rich basalts prevents crystallization of orthopyroxene at any pressure, is challenged by the results of Kinzler & Grove (1992*a*, 1992*b*). In addition, the high MgO contents of Icelandic picrites have recently been attributed to accumulation of 15–25 wt % olivine in basaltic melts with MgO ~12 wt % and *mg*-number ~72·8 (Revillon *et al.*, 1999), which is also the average composition of primitive melt inclusions found in Fo-rich olivines from picrites (Gurenko & Chaussidon, 1995). Finally, Slater *et al.* (2001) recently presented ample evidence for the existence of aggregated primary magmas with SiO_2 <49·7 wt % trapped as inclusions in Fo-rich (89–92) olivines generated in the mantle beneath Theistareykir, NE Iceland. In summary, based on major elements alone, the primary magma parental to the Kistufell magmas may be characterized as a primitive ol-tholeiite (MgO ~13·6 wt %, *mg*-number 72·5–72·8) derived by polybaric melting of a depleted mantle source (e.g. Kinzler & Grove, 1992*b*).

Estimates of pressure and temperature

It is argued below that the Kistufell magma equilibrated and started crystallizing at a high average pressure before eruption. The majority of the samples project between the 10 kbar and 15 kbar ol + cpx + (spi) + liq cotectic in the An–Ol–Si pseudo-liquidus phase diagram (Elthon, 1983) (Fig. 10). Likewise, the Cr-spinel microphenocryst inclusions in olivine could have equilibrated with the melt at a similar pressure range (Sobolev & Danyushevsky, 1994) (Fig. 11), such as already indicated by the SPINMELT modelling (Fig. 3). As this pressure corresponds to the base of the crust (~30–40 km, Gebrande *et al.*, 1980; Bjarnason *et al.*, 1993; Menke *et al.*, 1996; Staples *et al.*, 1997; Menke, 1999; Darbyshire *et al.*, 2000) it cannot represent a meaningful melting pressure. However, the fractionation-corrected composition (nal606 + 4% ol) projects between the 15 kbar and 20 kbar cotectic (Fig. 10), which may indicate the range of pressures at which the Kistufell magma was generated. This is in accordance

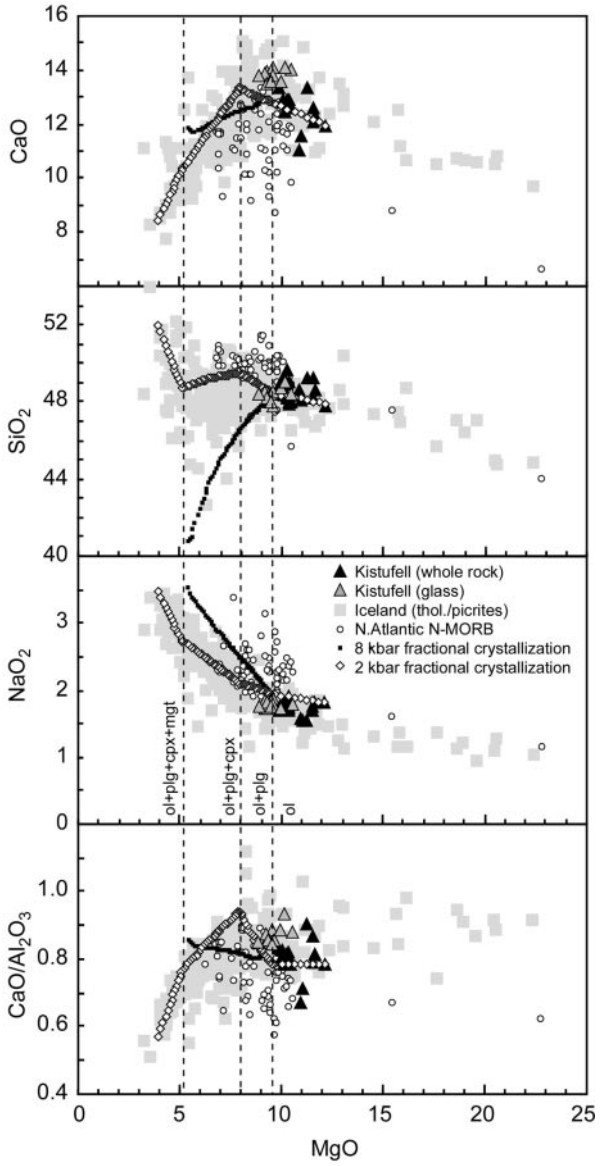

Fig. 5. Whole-rock and glass major element compositions of Kistufell samples. Shown for comparison are data for: Icelandic tholeiites and picrites (Wood *et al.*, 1979; Elliott *et al.*, 1991; Nicholson & Latin, 1992; Hemond *et al.*, 1993; Gurenko & Chaussidon, 1995; Hardarson *et al.*, 1997; Slater *et al.*, 1998) and North Atlantic N-MORB, which includes Leg 152 (Fitton *et al.*, 1998*b*), Hatton Bank (Brodie & Fitton, 1998), Gakkel Ridge (Mühe *et al.*, 1993, 1997) and the Mid-Atlantic Ridge from 36 to 53°N (Sun *et al.*, 1975; Presnall & Hoover, 1978; Schilling *et al.*, 1983). Fractional crystallization models (2 and 8 kbar) were evaluated using COMAGMAT (Ariskin *et al.*, 1993) at 0·1 wt % H_2O and $Fe^{2+}/Fe^{total} = 0{\cdot}9$, calculating equilibrium compositions in steps of 1 vol. %. Fractionation of olivine is followed by ol + plg, ol + plg + cpx, ol + plg + cpx + mgt at 2 kbar, or opx + cpx + plg, opx + cpx + plg + mgt at 8 kbar. Fractionation of a new phase is often marked by inflections in the model trends.

with rare earth inversions, which suggest that the highest melt production per kilobar decompression is at similar pressures (e.g. Slater *et al.*, 1998).

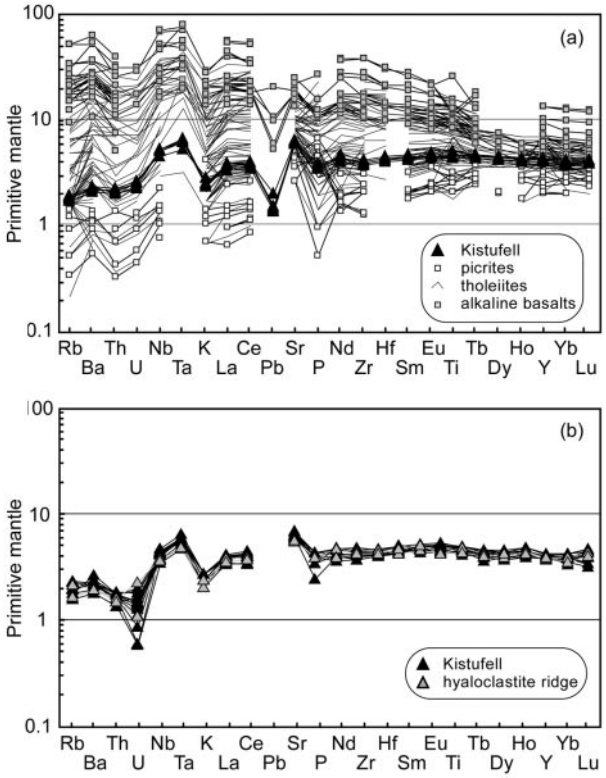

Fig. 6. Primitive mantle normalized (McDonough & Sun, 1995) trace element concentrations of Kistufell glass shards (a) Durham data (GEUS samples) and (b) Vandoeuvre data (nal samples). The two datasets show very similar results, except that three points indicate some analytical uncertainty with respect to the Vandoeuvre data: (1) the normalized values of U, Th, Rb, Ba and Lu vary considerably; (2) the normalized U and Th values are consistently lower than the Durham data; (3) the HREE shows a rather jagged pattern. The conclusions are therefore based mainly on the Durham data. Both datasets show depletion of large ion lithophile elements (LILE), negative Pb anomaly, and consistent positive Nb, Ta and Sr anomalies on the otherwise smooth normalized patterns. Picrites, tholeiites and alkaline basalts (Wood *et al.*, 1979; Elliott *et al.*, 1991; Furman *et al.*, 1991; Hemond *et al*, 1993; Gurenko & Chaussidon, 1995; Hards *et al.*, 1995; Hardarson *et al.*, 1997; Slater *et al.*, 1998) generally show similar features, although alkaline basalts do not show LILE depletion and Sr anomalies. It should be noted that the trace element chemistry of Kistufell and the hyaloclastite ridge (Vandoeuvre data) varies within the analytical uncertainty (see text for explanation).

Olivine–glass thermometry (Leeman, 1978) indicates eruption temperatures up to 1240°C (Ol_{rim}–glass: 1188–1240°C). This is similar to the highest values found elsewhere in the rift zone (1130–1230°C) (Mäkipää, 1978*a*; Werner, 1994; Schiellerup, 1995) and to those obtained from studies of primary melt inclusions in olivine from primitive ol-tholeiites and picrites in Iceland (1230–1240°C: Hansteen, 1991; Gurenko & Chaussidon, 1995; Hansen & Grönvold, 2000). These values demarcate minimum quenching temperatures of primary melt inclusions, as well as maximum eruption temperatures of ol-tholeiitic basalts close to mantle equilibrium, and are thought to monitor conditions prevailing

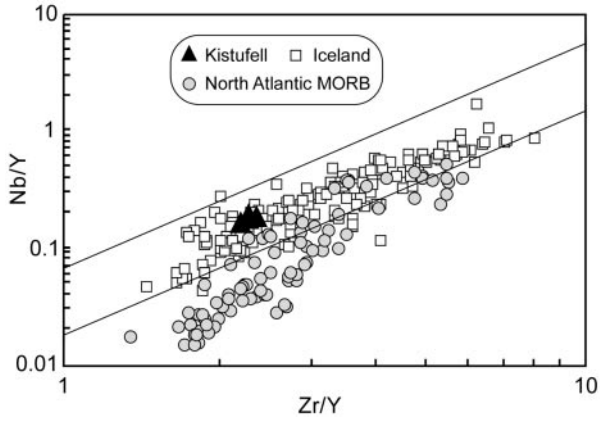

Fig. 7. Nb/Y vs Zr/Y for Icelandic lavas (Wood *et al.*, 1979; Schilling *et al.*, 1983; Elliott *et al.*, 1991; Furman *et al.*, 1991; Nicholson & Latin, 1992; Hemond *et al*, 1993; Gurenko & Chaussidon, 1995; Hards *et al.*, 1995; Hardarson *et al.*, 1997; Gunnarsson *et al.*, 1998; Slater *et al.*, 1998) and North Atlantic MORB (Gariepy *et al.*, 1983; Morton *et al.*, 1988, 1995; Mühe *et al.*, 1993, 1997; Brodie & Fitton, 1998; Fitton *et al.*, 1998*b*). Parallel lines highlight the 'Iceland' field of Fitton *et al.* (1997).

at the mantle–crust boundary (e.g. Hansteen, 1991). In conclusion, *P–T* estimates suggest that the Kistufell magma last equilibrated at the base of the Icelandic crust and passed through the crust with minimum heat loss, thereby constraining the amount and type of contamination that can be expected.

Evidence for crustal contamination?

Hydrothermal interaction

Post-eruption alteration may explain the excess Sr concentrations and the uniquely low $\delta^{18}O$ values found in some Icelandic lavas (Hemond *et al.*, 1993; Chauvel & Hemond, 2000), because hydrothermal fluids in Iceland are characterized by high concentrations of mobile elements (Sr, Rb, Ba) (Olafsson & Riley, 1978) and low $\delta^{18}O$ values (e.g. −11·9‰, Sveinbjörnsdottir *et al.*, 1986). This can, however, be excluded in the case of Kistufell because only fresh glass shards were analysed, the $\delta^{18}O$ values are essentially constant varying within the

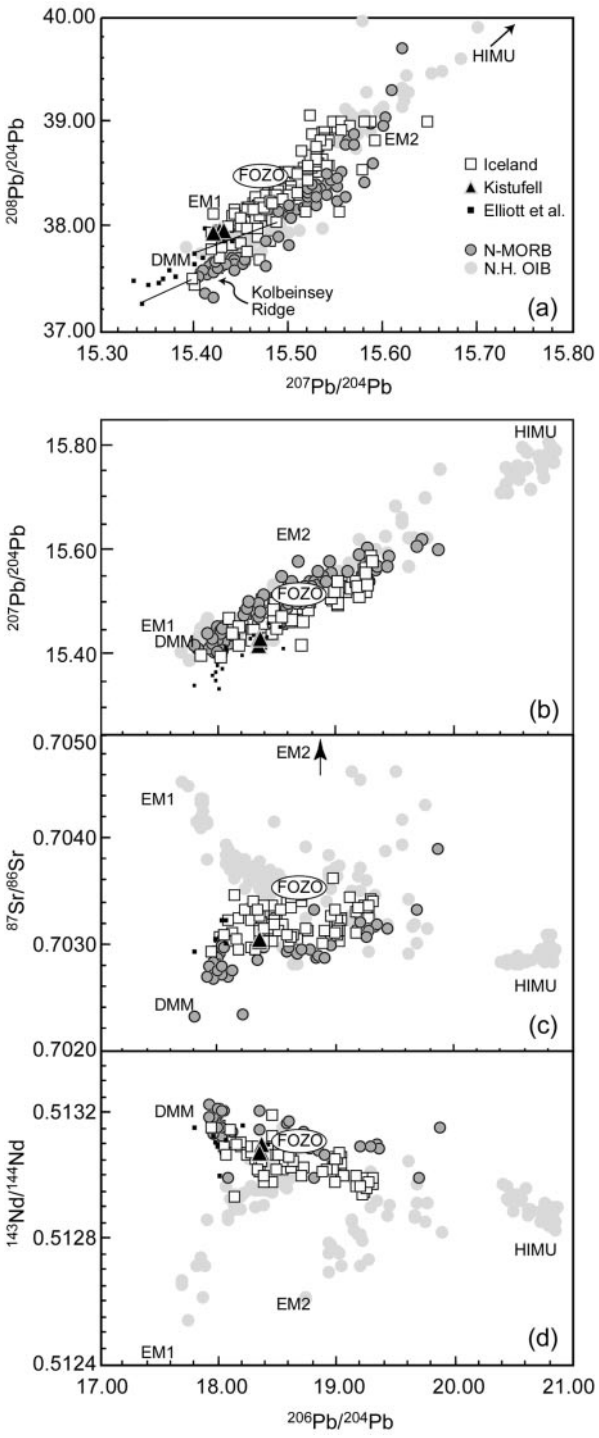

Fig. 8. (a)–(d) Pb, Sr and Nd isotopic variation in Iceland basalts and North Atlantic MORB. North Atlantic MORB, compared with Northern Hemisphere OIB (N.H. OIB), is mainly from 34°N to 53°N, but includes data from 67·3°N–69·7°N and 85°N–86°N (Cohen *et al.*, 1980; Dupré & Allègre, 1980; Ito *et al.*, 1987; Mertz *et al.*, 1991; Frey *et al.*, 1993; Mühe *et al.*, 1993, 1997; Schilling *et al.*, 1999). Iceland data are from Sun & Jahn (1975), Sun *et al.* (1975), Cohen & O'Nions (1982), Park (1990), Elliott *et al.* (1991), Furman *et al.* (1991), Hards *et al.* (1995), Hanan & Schilling (1997), Hardarson *et al.* (1997), Stecher *et al.* (1999) and Chauvel & Hemond (2000). N.H. OIB includes Hawaiian Islands, the Azores, Cape Verde and Fernando de Noronha (Staudigel *et al.*, 1984; Stille *et al.*, 1986; Gerlach *et al.*, 1987, 1988; Hart, 1988; Davies *et al.*, 1989; Roden *et al.*, 1994; Rhodes & Hart, 1995; Sims *et al.*, 1995; Bennett *et al.*, 1996; Hauri *et al.*, 1996; Valbracht *et al.*, 1996; Lassiter & Hauri, 1998). Values for EM1, EM2, HIMU and DMM are taken from Saunders *et al.* (1988), and St. Helena is further included for HIMU reference (Chaffey *et al.*, 1989). Replicate data of Elliott *et al.* (1991) and Hanan & Schilling (1997) are connected by lines.

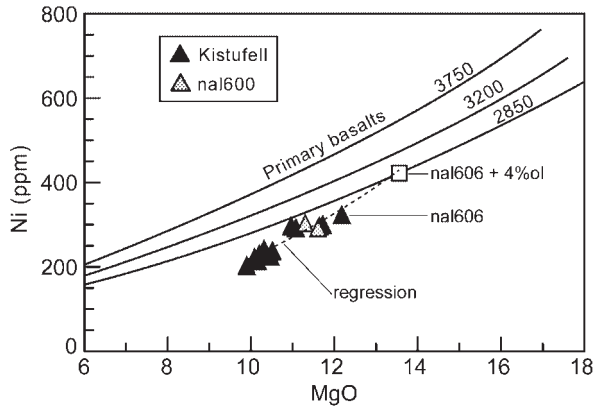

Fig. 9. Ni (ppm) vs wt % MgO. Curves represent primary basalts in equilibrium with mantle olivines of varying Ni content (in ppm) (Elthon, 1987). Presumably some olivine fractionation (~4 wt %) has occurred since the Kistufell magma (nal606) was in equilibrium with mantle olivine. The intersection between the fractionation trend [which can be approximated by a regression line (dashed) as long as olivine is the only liquidus phase] and the line representing liquids in equilibrium with mantle olivine (2850 ppm Ni) corresponds to a 'primary' composition. The same composition can be independently calculated by adding 4% ol to nal606.

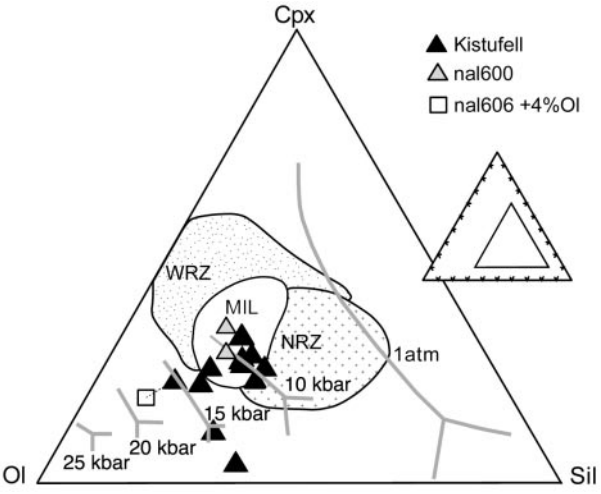

Fig. 10. CMAS isomolar projections in pseudo-liquidus phase diagram (Elthon, 1983, 1989). Equilibrium curves from Elthon (1983). Insert shows position of diagram: apices of the triangle are $Ol_{60}An_{15}Sil_{25}$ (left), $An_{65}Ol_{10}Sil_{25}$ (top), $Sil_{75}An_{15}Ol_{10}$ (right). The bulk of the samples plot close to the 10 kbar (pseudo)-eutectic, representative of ol-tholeiites throughout Iceland. Shaded fields represent data from Western Rift Zone (WRZ), Northern Rift Zone (NRZ) and Mid-Iceland Belt (MIL) (Hemond *et al.*, 1993). Samples having higher normative olivine plot towards the highest pressures. Fractionation corrected nal606 + 4% ol (Fig. 8) plots between the 15 kbar and 20 kbar ol–cpx–sp–liq cotectic line.

analytical uncertainty, the other mobile elements (Rb, Ba) do not show spikes on the normalized trace element abundance patterns (Fig. 6), and there is no geothermal activity in the area.

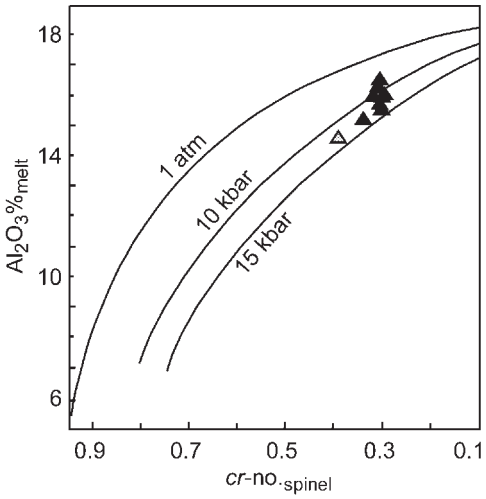

Fig. 11. Pressure dependence of spinel composition (*cr*-number) vs wt % Al_2O_3 in the equilibrium melt after Sobolev & Danyushevsky (1994). Kistufell Cr-spinels plot between 10 and 15 kbar pressure, consistent with the CMAS projections (Fig. 10). Although pressure is generally believed to affect the *cr*-number in MORB spinels (Dick & Bullen, 1984; Fujii & Scarfe, 1985; Falloon & Green, 1987; Natland, 1989), the results of Roeder & Reynolds (1991) do not show clear relations between *cr*-number and pressure. It should be noted that correcting melt compositions for incipient olivine fractionation will decrease the Al_2O_3% to ~95% of the value and thus not change the main conclusions.

Given the general correlation between proximity to central volcanoes, degree of evolution, increasing $^{87}Sr/^{86}Sr$ and decreasing $\delta^{18}O$ amongst Icelandic basalts (Hemond *et al.*, 1988; Nicholson *et al.*, 1991; Sigmarsson *et al.*, 1991; Jónasson, 1994; Gunnarsson *et al.*, 1998), the most plausible contamination mechanism involves heat-releasing crystallization in magma reservoirs beneath central volcanoes and assimilation of hydrothermally altered low $\delta^{18}O$ crust, enriched in mobile elements. The effects of assimilation of hydrothermally altered metabasalts are examined below.

Crustal assimilation

Assimilation processes may be viewed on the scale of both the entire rift zone and individual volcanic centres. On a regional scale, the continuous subsidence, hydration and progressive metamorphism of the rift zone rocks has the potential to generate mineral assemblages that are fusible at temperatures prevailing in the lower crust. It has therefore been argued that variable mixing of crustal anatectic melts and primary magmas from a homogeneous mantle source may account for the entire petrological diversity in Iceland (Oskarsson *et al.*, 1982, 1985; Steinthorsson *et al.*, 1985; Hemond *et al.*, 1988). Although this model does not account for the isotopic variation in Iceland (Hemond *et al.*, 1993), it illustrates the potential of assimilation processes in modifying primary magma

compositions. Interestingly, apart from a few depleted picrites and ol-tholeiites ($^{87}Sr/^{86}Sr$ <0·7031), fresh Icelandic volcanics are rarely in equilibrium with normal peridotite mantle and have exceptionally low $\delta^{18}O$ values (1·0–6·2‰) compared with basalts elsewhere (Muehlenbachs *et al.*., 1974; Hattori & Muehlenbachs, 1982; Oskarsson *et al.*, 1982; Condomines *et al.*, 1983; Hemond *et al.*, 1988, 1993; Nicholson *et al.*, 1991; Sigmarsson *et al.*, 1992; Gee *et al.* 1998*b*; Gunnarsson *et al.*, 1998). The lowest ratios are observed in felsic rocks and qz-tholeiites from volcanic centres (Muehlenbachs *et al.*, 1974; Nicholson *et al.*, 1991; Sigmarsson *et al.*, 1991) and are attributed to assimilation or melting of crust, hydrothermally altered by low $\delta^{18}O$, high-latitude meteoric water at high temperatures. The low $\delta^{18}O$ in picrites and ol-tholeiites are therefore often interpreted as a result of similar, but less extensive, processes.

The importance of assimilation processes has mainly been demonstrated from the composition of lavas erupted from the Icelandic central volcanoes, and such processes have been suggested to occur most notably at local magma chambers where magmas may reside for relatively long periods of time (e.g. Condomines *et al.*, 1983; Nicholson *et al.*, 1991; Sigmarsson *et al.*, 1991, 1992; Nicholson & Latin, 1992; Hemond *et al.*, 1993; Jónasson, 1994). They may, however, seem more widespread than they actually are, because long distance (up to 100 km) lateral flow of magmas from volcanic centres into associated dyke swarms is a common process in Iceland (Sigurdsson & Sparks, 1978; Blake, 1984; McGarvie, 1984; Helgason, 1989; MacDonald *et al.*, 1990).

The petrology of the Kistufell samples studied here provides conflicting information as to whether crustal assimilation has a major role in affecting the primary magma compositions. The unfractionated major element composition, extremely reduced iron, high $^{3}He/^{4}He$ ratios, uniform and low Sr and Pb (and high Nd) isotopic ratios, and depleted incompatible trace element patterns, all indicate a limited role for processes involving assimilation of crustal rocks. The phenocryst mineral assemblage, mineral chemistry and low crystallinity further suggest that crystallization was restricted after the Kistufell magma segregated from the mantle. There is no evidence of crystallization episodes between the formation of olivine phenocrysts in equilibrium with a mantle-derived parent magma and microphenocrysts in equilibrium with the erupted melt. Despite these circumstances, three observations, potentially, can be interpreted as indicating that crustal-level processes did occur: (1) the small population (1 vol. %) of olivine, plagioclase and Cr-spinel macrocrysts, which are not in equilibrium with the host glass and all display complex or reverse zoning (Figs 2a and b and 3); (2) the anomalous Sr concentrations (Fig. 6); (3) the low oxygen isotopic ratios (see Fig. 13, below).

The disequilibrium macrocrysts are thought to be xenocrysts derived by incorporation of a minor volume of solid crustal rocks, or olivine–spinel–plagioclase-saturated melt, into the Kistufell magma. This model most readily explains the reverse zoning in xenocrysts of plagioclase and olivine, combined with the completely regular zoning in olivine phenocrysts (e.g. Sigurdsson, 1981; Meyer *et al.*, 1985; Niu & Batiza, 1994; Hansen & Grönvold, 2000). Magmatic differentiation at fluctuating pressure and water pressure could in theory produce reverse zoning in olivine and plagioclase, but cannot explain the observed zonation towards higher *mg*-number and lower *cr*-number in the Cr-spinel phenocrysts (Figs 4 and 5a), unless considerable amounts of Cr-spinel crystallized unaccompanied by other phases. This is considered unlikely. Pressure variations cannot account for these variations, as crystallization during pressure release would produce the opposite zonation (Sobolev & Danyushevsky, 1994). The reverse or complex zonation is thus thought to reflect incorporation of evolved Cr-spinel, olivine and plagioclase xenocrysts into the plagioclase-undersaturated Kistufell magma while this was passing through the crust. The total amount of entrained material cannot be deduced, because some of it may have been partially melted, but it is important to note that the present xenocrysts cannot alone substantiate a serious contamination hypothesis, because their amount is insignificant.

Because the Kistufell glass compositions can be related to a primary magma by small amounts of crystallization (<4% ol) the potential proportion of assimilated material is likely to be small. Therefore, to account for the marked change in $\delta^{18}O$ values and Sr contents, the assimilated material would have to be of a rather extreme composition. In theory, addition of 5% highly altered wall rock with $\delta^{18}O \sim -10‰$ and ~800 ppm Sr could produce a Kistufell-like magma composition from a primary magma with $\delta^{18}O$ +5·5‰ and ~90 ppm Sr. Evidence from drill holes at Krafla verifies that highly depleted $\delta^{18}O$ values occur (–3·4 to −10·5‰, Hattori & Muehlenbachs, 1982). However, such a low $\delta^{18}O$ crust is not ubiquitous and these values are much lower than those of rhyolites and dacites regarded to represent the average depletion [$\delta^{18}O = +2(\pm 1)‰$] of the hydrothermally altered crust (Gautason & Muehlenbachs, 1998).

Given the relatively large distance from Kistufell to the nearest volcanic centres and the absence of geothermal activity, any potential assimilation processes must be assumed to operate at deep crustal levels beneath Kistufell. This is important because whereas meteoric waters in the upper crust may have low $\delta^{18}O$, fluids in the deeper parts of the crust are expected to have $\delta^{18}O$ from +4‰ to +5‰ because they invariably equilibrate with the crust (Hemond *et al.*, 1993). If this is the case,

assimilation of very large proportions of crust (50–80 vol. %) is necessary to generate the observed oxygen isotopic ratios, which is clearly inconsistent with the primitive nature of the Kistufell magmas and the notable absence of positive spikes in the trace element patterns at all mobile elements except Sr (Fig. 6).

Selective contamination may, in theory, explain the elevated Sr abundances and low $\delta^{18}O$ values, because almost any combination of primary and secondary phases in the heterogeneous Icelandic crust can be argued to have contaminated the Kistufell magmas along their pathway through the crust. Thus a contaminant, or a sequence of contaminants, with a total effect only on $\delta^{18}O$ and Sr, could possibly be hypothesized. However, in reality, contamination would probably affect other elements as well. The potential Sr hosts in chlorite–epidote facies and greenschist facies upper crust are carbonate, or epidote, which may contain up to 1 wt % Sr (Exley, 1982). In amphibolite and granulite facies lower crust, calcic plagioclase replaces the original igneous plagioclase and may host the Sr (Drake & Weill, 1975). However, assimilation of epidote and other secondary minerals such as prehnite, calcite, biotite, garnet, diopside, augite, calcic plagioclase and various amphiboles would cause introduction of K, Na, Sr, Rb and Ba, and significant amounts of Ca and Fe^{3+}, which may constitute up to 33 wt % of these minerals (Exley, 1982). Similarly, assimilation of lower-crustal lithologies would probably also involve endiopside, shifting Al_2O_3/CaO towards high ratios as observed in many picrites (Trønnes, 1990; Hansteen, 1991) and yet Al_2O_3/CaO ratios are not different from those for other basalts at a given MgO content (Fig. 5) and there is no enrichment of Fe^{3+}, K, Na, Rb and Ba.

In conclusion, the Kistufell basalts are contaminated, as verified by the presence of a very small amount of xenocrysts. The effects of contamination are, however, insignificant and the low $\delta^{18}O$ values and excess Sr abundances are considered to be unrelated to contamination. Selective assimilation of secondary minerals is an unlikely explanation, as it is questionable how crustal processes can significantly affect O and Sr in a primitive magma without affecting abundances or ratios of other elements. Direct interaction between magma and deep-seated surface-derived fluids may be an option; the potential mechanism at work is, however, unclear (Gautason & Muehlenbachs, 1998). It is therefore suggested that Kistufell is essentially uncontaminated and that the anomalous chemical signatures, such as low $\delta^{18}O$ values and excess Sr, are inherited from the source.

The depleted plume component of Kistufell

Trace element characteristics

Negative Pb anomalies and positive Nb and Ta anomalies, such as observed in the Kistufell basalts, are general features of OIBs but can also be found at a reduced level in MORB (e.g. Hofmann *et al.*, 1986; Hofmann & Jochum, 1996; Hofmann, 1997). They have been attributed to dehydration and melting processes during subduction, producing a Pb-depleted, Nb-enriched recycled oceanic lithosphere component, which may eventually become the source of OIB (Hofmann & White, 1982; Saunders *et al.*, 1988; Weaver, 1991; Chauvel *et al.*, 1995; Stalder *et al.*, 1998). Pb concentration data are sparse for Icelandic basalts; strongly negative anomalies, however, characterize picrites, ol-tholeiites and alkaline basalts (Elliott *et al.*, 1991; Hards *et al.*, 1995; Hardarson *et al.*, 1997). Excess Nb in Icelandic basalts relative to global N-MORB has been suggested from Nb/U ratios (Hemond *et al.*, 1993) and logarithmic plots of Nb/Y vs Zr/Y (Fitton *et al.*, 1997; Saunders *et al.*, 1997). Kistufell basalt data plot close to the Nb-enriched mantle composition hypothesized by Fitton *et al.* (1997) and well inside the depleted part of the Iceland array, where the deviation from North Atlantic N-MORB is largest (Fig. 7). The ubiquitous presence of Nb and Pb anomalies in the entire suite of Icelandic basalts may be indicative of a large proportion of recycled oceanic lithosphere in the plume. For instance, the K/Nb [166–187 (223)], La/Nb (0·69–0·74) and Zr/Nb (12–13) ratios (ICP-MS) in Kistufell are much closer to typical HIMU basalts (K/Nb 77–179, La/Nb 0·66–0·77, Zr/Nb 3–5) than to N-MORB (K/Nb 296, La/Nb 1·1, Zr/Nb 30) [HIMU and N-MORB values from Weaver (1991)].

The excess Sr in Icelandic tholeiites, picrites and ultraprimitive melt inclusions could be interpreted in terms of plagioclase assimilation (Sobolev *et al.*, 1994) or melting in the plagioclase stability field (Gurenko & Chaussidon, 1995; Gee *et al.*, 1998*b*), rather than by contamination with hydrothermally altered crust (Hemond *et al.*, 1993). The plagioclase assimilation model, however, fails because the required amounts would result in unusually high Al_2O_3 contents, which are not observed (see Hemond *et al.*, 1993; Gee *et al.*, 1998*b*). The melting model has the advantage that it explains why primitive Icelandic alkaline basalts do not exhibit excess Sr, as opposed to a contamination model, which does not. However, it does not explain the occurrence of positive Sr spikes in primitive ol-tholeiites erupted in central Iceland, where the base of the crust is considerably below the plagioclase stability field (Gebrande *et al.*, 1980; Bjarnason *et al.*, 1993; Menke *et al.*, 1996; Staples *et al.*, 1997; Menke, 1999). A melting model also faces the problem that the high degrees of melting should have nearly exhausted the mantle source and any additional melting in the upper few kilometres of the melting column will have little effect on the bulk melt composition. Indeed, decompression melting is likely to end if the upwelling mantle crosses the spinel–plagioclase peridotite transition

(Asimov *et al.*, 1995) and is thus not an obvious explanation.

A third option is that the Sr anomaly in Icelandic high-degree melts is a primary feature related to the presence of a distinct, refractory mantle component, as also recently suggested for Hawaii (Hofmann, 1999; Sobolev *et al.*, 2000). This explains its absence in low-degree alkaline melts, which probably are generated from the more fertile parts of the rising plume. It also explains its presence in high-degree melts generated at depths below the plagioclase stability field. Because the entire range of basaltic melts in Iceland bear explicit signs of a recycled component, but only high-degree melts exhibit excess Sr, this is thought to be associated with heterogeneity in the recycled component. Indeed, Chauvel & Hemond (2000) have suggested that Icelandic high-degree melts are generated by partial melting of a refractory plume component comprising subduction zone processed, recycled oceanic gabbros, whereas low-degree melts are primarily generated from recycled oceanic basalts that are more fertile. Kilometre-scale chemical heterogeneities have previously been suggested to be preserved over long periods of time in the convecting mantle (Shimizu *et al.*, 1999; Sobolev *et al.*, 1999), and melting of different lithological units of recycled oceanic lithosphere has also been inferred to explain the geochemical variability of Hawaiian basalts (Lassiter & Hauri, 1998). If this is the case, recycled lower-crustal gabbros may be the source of the excess Sr, as their *in situ* equivalents possess strongly elevated Sr abundances relative to other trace elements (Dick *et al.*, 1991; Werner, 1997). Although excess Sr has been ascribed to changes in partitioning behaviour (Blundy & Green, 2000) or melting of ultra-depleted mantle components without the presence of metagabbros (Lundstrom *et al.*, 1998), the recycling scenario is favoured here. This is because it better explains the strong positive correlation between Sr_n/Nd_n and $^{143}Nd/^{144}Nd$ (Fig. 12), as the recycled basaltic and gabbroic sequences should have not only different Sr_n/Nd_n, but also different isotopic signatures, developed since their initial formation.

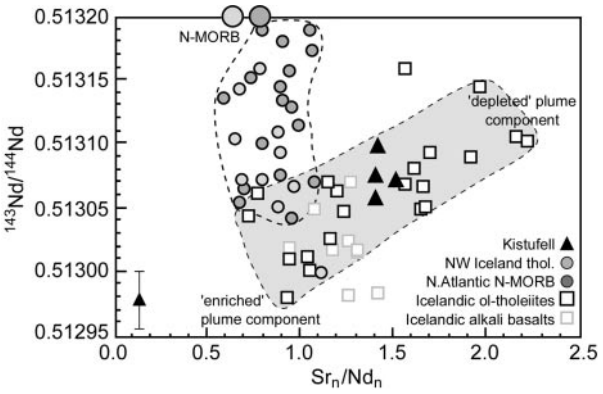

Fig. 12. $^{143}Nd/^{144}Nd$ vs Sr_n/Nd_n for Icelandic basalts (Furman *et al.*, 1991; Hards *et al.*, 1995; Hardarson *et al.*, 1997; Gee *et al.*, 1998*a*; Chauvel & Hemond, 2000) and North Atlantic N-MORB including basalts from Knipovich Ridge, Kolbeinsey Ridge and the SE Greenland margin (Neumann & Schilling, 1984; Devey *et al*, 1994; Fitton *et al.*, 1998*a*). N-MORB values (large circles) are from Saunders *et al.* (1988), Hofmann (1988) and Sun & McDonough (1989). The data are MgO-screened (MgO >6 wt %) to minimize the influence of plagioclase fractionation on the Sr_n/Nd_n ratio, which measures excess Sr in the basalts. Only ICP-MS data, isotope dilution data or high-quality XRF data (long counting times) have been included for Iceland. Although plume-derived ol-tholeiites (shaded field) have $^{143}Nd/^{144}Nd$ comparable with North Atlantic MORB (white field), they are clearly discernible on the basis of their excess Sr (high Sr_n/Nd_n). It should be noted that North Atlantic MORBs are clearly influenced by an enriched plume component and, in contrast, NW Iceland tholeiites are clearly influenced by the MORB-source, consistent with the interpretation by Hardarson *et al.* (1997). Recycled gabbros are suggested to constitute part of the 'depleted' component. Recycled basalts may constitute the 'enriched' component that source Icelandic alkali basalts (Chauvel & Hemond, 2000); it is, however, likely that the FOZO component, which has low $^{143}Nd/^{144}Nd$ (0·51297, Hilton *et al.*, 1999), has Sr_n/Nd_n close to unity. These two components are thus not discernible in this diagram.

Lead, strontium and neodymium isotopic characteristics

It has been advocated that the isotopically depleted component in the source of Icelandic basalts is a depleted North Atlantic MORB source component entrained in the plume (e.g. Sun *et al.*, 1975; Mertz & Haase, 1997; Hanan *et al.*, 2000). However, both isotopically depleted and enriched Icelandic basalts are offset from North Atlantic MORB in a diagram of $^{208}Pb/^{204}Pb$ vs $^{207}Pb/^{204}Pb$ (Fig. 8a). This has led to the suggestion that a distinct depleted component is an integral part of the plume (Hards *et al.*, 1995; Kerr *et al.*, 1995; Thirlwall, 1995) and that it could be a 0·2–1·2-Gy-old recycled component (Thirlwall *et al.*, 1998). Mertz & Haase (1997), however, reported substantial overlap in Pb, Sr and Nd isotopic composition between Icelandic basalts and depth-filtered (< -2500 m) North Atlantic MORB between 34°N and 53°N and found no evidence for the above scenario. The entire overlap is, however, due to the Pb, Sr and Nd isotopic ratios in ~35°N MORBs, which have been reported elsewhere to be influenced by the plumes responsible for the Azores and the New England Seamounts (Shirey *et al.*, 1987). Accordingly, these samples cannot be considered typical North Atlantic MORB and general involvement of North Atlantic MORB source material in Icelandic lavas is therefore not demonstrated.

Kistufell plots close to the unradiogenic endmember of the Iceland array in the $^{208}Pb/^{204}Pb$ vs $^{207}Pb/^{204}Pb$ diagram (Fig. 8a). Few Icelandic rocks have less radiogenic Pb than Kistufell (Fig. 8a) and these appear to be derived, at least in part, from a North Atlantic N-MORB source. Tertiary tholeiites from NW Iceland have already been related to this source on the basis of trace element ratios and Pb isotopes (Hardarson *et al.*, 1997). Additionally, it seems that the Pb isotope compositions

of the Reykjanes and Theistareykir picrites reported by Elliott *et al.* (1991) are erroneous and underwent substantial mass fractionation in the mass spectrometer, as replicate analyses gave significantly more radiogenic values (Hanan & Schilling, 1997; Thirlwall *et al.*, 1998; Thirlwall, 2000). The new values fall close to the MORB array (Fig. 8a), as is also the case with the original Sr and Nd isotopic ratios (Fig. 8c and d) (Elliott *et al.*, 1991). To the extent that the Sr–Nd–Pb isotopes distinguish the present mantle components, it can be argued that influx, and partial melting, of ambient upper mantle may occur in parts of the neovolcanic rift zone, which are distant from the plume axis. Whether this material derives from shallow-level influx of upper DMM material or from a sheath of DMM material entrained near the 670 km discontinuity, as proposed by Kempton *et al.* (2000), is beyond the scope of this paper. Here, the important point is that Kistufell has Pb isotopic compositions close to a well-defined unradiogenic component, which is different from the North Atlantic N-MORB source, and that other depleted signatures are absent above the plume axis.

A clearer distinction between DMM and the depleted plume component is provided in Fig. 12, in which DMM (Sr_n/Nd_n ~0·64–0·77, $^{143}Nd/^{144}Nd$ ~0·5132) plots far from the Iceland field of variation (DMM values: Hofmann, 1988; Saunders *et al.*, 1988; Sun & McDonough, 1989). Only basalts with MgO >6 wt % are included in this diagram, to minimize the effects of plagioclase fractionation on the Sr_n/Nd_n ratio. Icelandic basalts and local N-MORB (Kolbeinsey Ridge, Knipovich Ridge, Leg 152) clearly constitute diverging arrays in this diagram. The influence of a DMM component in the source of tholeiites from NW Iceland is clearly illustrated by the isolated data array, which also strongly diverges from the main Iceland trend (Fig. 12). The NW Iceland tholeiites were previously inferred to derive partly from a DMM source on the basis of ΔNb and Pb isotope data (Hardarson *et al.*, 1997). A few high $^{143}Nd/^{144}Nd$ picrites from Reykjanes Peninsula (Gee *et al.*, 1998*b*) appear to trail off the tip of the Iceland trend towards N-MORB and may be influenced by DMM in a similar way. Kistufell plots well within the array of Icelandic basalts and shows no resemblance to basalts with DMM source characteristics. In conclusion, the source of Kistufell and other primitive basalts that are situated directly above the plume stem (Chauvel & Hemond, 2000) derives from partial melting of a depleted mantle component, different from that which sources North Atlantic MORB.

Oxygen and helium isotopic signatures

As previously noted, the prevalence of low $\delta^{18}O$ tholeiites in Iceland may indicate that assimilation and exchange processes are extremely effective in overprinting the isotopic characteristics of the primary magmas, or alternatively that low $\delta^{18}O$ mantle exists beneath Iceland, as also proposed for Hawaii (Eiler *et al.*, 1996; Lassiter & Hauri, 1998). Values equivalent to $\delta^{18}O$ ~3·5–4·5‰ were recently inferred for an intrinsic Iceland plume component on the basis of correlating $\delta^{18}O$ and $^{143}Nd/^{144}Nd$ isotopic compositions in Reykjanes Ridge basalts (Thirlwall *et al.*, 1999). Such ratios can be reconciled with a recycling model, because altered oceanic gabbros often have low $\delta^{18}O$ values (Kempton *et al.*, 1991).

In detail, O and Sr isotopic data for Icelandic lavas plot in a roughly triangular array, which may be explained by mixing of three components: depleted MORB mantle (DMM), hydrothermally altered Icelandic crust, and homogeneous, relatively undegassed lower mantle (Fig. 13). This traditional model ascribes the petrogenesis of Icelandic alkali basalts to partial melting of a lower-mantle component (e.g. Hemond *et al.*, 1993). It is useful, however, to consider the $^3He/^4He$ systematics in this context, because the relatively low $^3He/^4He$ in Icelandic alkali basalts and high $^3He/^4He$ in some ol-tholeiites (Kurz *et al.*, 1985; Sigmarsson *et al.*, 1992; Wiese, 1992; Breddam *et al.*, 2000) contradicts the traditional model. If, instead, alkali basalts are melt products of recycled basalts, they could be expected to have relatively low $^3He/^4He$, high $^{87}Sr/^{86}Sr$ and mantle $\delta^{18}O$ values, as observed. Because recycled basalts are expected to be relatively rich in ^4He produced by Th and U decay (Moreira & Kurz, 2001), their $^3He/^4He$ isotopic signature should be low and relatively hard to overprint by the high $^3He/^4He$, lower-mantle component in the plume. In contrast, oceanic gabbros have lower amounts of He, Th and U and their recycled equivalents are therefore more easily overprinted by the lower-mantle component. Conversely, the Sr isotopic composition of the recycled gabbros is hard to alter because they are about 10 times richer in Sr than is primitive mantle. This could explain the decoupling of He isotopes from other isotopic systems; for example, the combination of high $^3He/^4He$ and low $^{87}Sr/^{86}Sr$ ratios in ol-tholeiitic basalts and moderate $^3He/^4He$ and high $^{87}Sr/^{86}Sr$ ratios in alkaline basalts, in Iceland (Condomines *et al.*, 1983; Sigmarsson *et al.*, 1992; this study).

It is hypothesized here that plume-derived Icelandic basalts have $\delta^{18}O$ and $^{87}Sr/^{86}Sr$ signatures corresponding to various mixtures of recycled basalt, recycled gabbro and a lower-mantle component (Fig. 13). It is therefore useful to briefly inspect the differences between the extrusive and intrusive lithological units of the well-characterized Oman ophiolite. This is because these differences may persist during recycling and explain some of the observed chemical variation. In terms of the chemical parameters discussed above, the cumulative Oman gabbros have 10–100 times lower trace element abundances, low $^{87}Rb/^{86}Sr$ and $^{238}U/^{204}Pb$ ratios, and

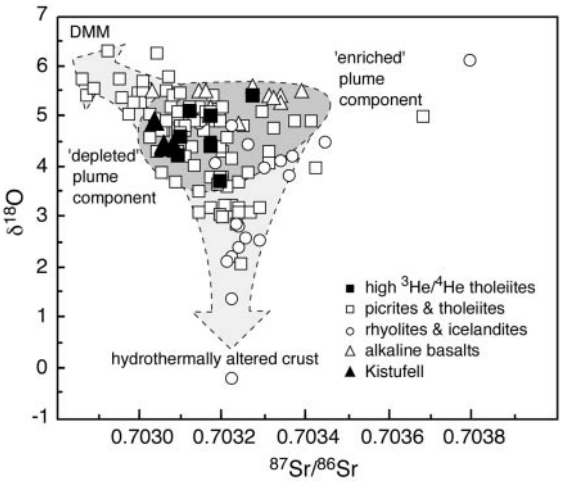

Fig. 13. $\delta^{18}O$ vs $^{87}Sr/^{86}Sr$ of Icelandic lavas (Oskarsson *et al.*, 1982; Condomines *et al.*, 1983; Nicholson *et al.*, 1991; Sigmarsson *et al.*, 1991, 1992; Nicholson & Latin, 1992; Hemond *et al.*, 1993; Gee *et al.*, 1998*a*; Gunnarsson *et al.*, 1998). Of the relatively small number of these samples that have been analysed for $^3He/^4He$ (Condomines *et al.*, 1983; Breddam *et al.*, 2000), those with values between 12 and 24 R/R_a have been highlighted (black). Olivine data have been recalculated to whole-rock equivalents for direct comparison with Kistufell, using a fractionation factor of 0·5.

high $^{147}Sm/^{144}Nd$ and Sr/Nd relative to the extrusive rocks (Chen & Pallister, 1981; McCulloch *et al.*, 1981; Benoit *et al.*, 1996). Down-section systematic differences also exist with respect to $\delta^{18}O$ values, which decline from 6–12‰ in the extrusive rocks to 3–6‰ within the gabbros (Gregory & Taylor, 1981; McCulloch *et al.*, 1981; Stakes *et al.*, 1984). Provided that such heterogeneity to some extent survives recycling, partial melts of recycled basalts can be inferred to have high $\delta^{18}O$ and $^{87}Sr/^{86}Sr$, and low $^{143}Nd/^{144}Nd$ and Sr_n/Nd_n ratios relative to recycled gabbros with sub-peridotitic $\delta^{18}O$, low $^{87}Sr/^{86}Sr$, and high $^{143}Nd/^{144}Nd$ and Sr_n/Nd_n ratios. The variation within the plume field in Fig. 13 could thus be consistent with various degrees of mixing between partial melts dominated by either recycled basalts or recycled gabbros (enriched and depleted plume component, respectively). In this scenario, the Sr isotopic signature of the recycled basalts is close to that of the lower mantle (FOZO), which is not unreasonable considering that the recycled basalts should develop more 'enriched' radiogenic isotope ratios than DMM. Finally, the low $\delta^{18}O$ and moderate $^{87}Sr/^{86}Sr$ values found in rhyolites and qz-tholeiites (Fig. 13) are attributed to assimilation of hydrothermally altered crust (e.g. Oskarsson *et al.*, 1982; Nicholson *et al.*, 1991; Sigmarsson *et al.*, 1991; Gunnarsson *et al.*, 1998). Conversely, mantle $\delta^{18}O$ values and low $^{87}Sr/^{86}Sr$ observed in ol-tholeiites from Reykjanes and Theistareykir (Hemond *et al.*, 1993; Gee *et al.*, 1998*b*) are ascribed to involvement of the DMM source (Fig. 13).

Mantle components in Iceland

In conclusion, the He, Sr, Nd and Pb isotopic ratios within primitive Icelandic lavas, including Kistufell, can be explained in terms of mixing between a refractory component equivalent to metagabbros and harzburgites of recycled oceanic lithosphere, and a FOZO-like component (Hilton *et al.*, 1999). In general, the isotope systematics in Iceland are therefore thought to be controlled by the composition of FOZO and a range of components with depleted to moderately enriched Sr, Nd and Pb isotopic ratios developed in the various units of recycled oceanic lithosphere during their residence time in the mantle. Recycled oceanic lithosphere may also include sediments responsible for the EM1 influence suggested by Hanan & Schilling (1997). The isotopic heterogeneity within the Iceland mantle plume may thus be viewed as a result of mixing between plume material rising from a layer of subducted slabs (which have partly maintained their geochemical integrity and heterogeneity) and lower-mantle material (FOZO) entrained in the initial stages of plume formation. This scenario is consistent with fluid dynamic and geochemical aspects of entrainment in mantle plumes (Hauri *et al.*, 1994; Farnetani & Richards, 1995). The source of North Atlantic MORB is not involved in the genesis of depleted ol-tholeiites in central Iceland. However, intermittent influx of DMM-like North Atlantic MORB source material in the periphery of the Iceland plateau (e.g. northernmost palaeo-rift zones, northernmost NRZ and the Reykjanes Peninsula) may still occur, as suggested from MORB-like trace element and Sr, Nd and Pb isotopic ratios (Hanan & Schilling, 1997; Hardarson *et al.*, 1997).

CONCLUSIONS

Kistufell is composed of the most primitive unaltered olivine tholeiitic glasses found above the plume axis in central Iceland and represents near-primary partial melts from the plume. The glasses represent virtually uncontaminated melts with 1% xenocrysts. Although excess Sr and low $\delta^{18}O$ values can potentially be ascribed to crustal assimilation, this interpretation is inconsistent with the depletion in Ba, Rb, K, Na, Fe, Ca and Si, low $^{87}Sr/^{86}Sr$, elevated $^3He/^4He$ ratios and the unfractionated nature of the rocks. The observed combination of high $^3He/^4He$ (15·3–16·8 R/R_a) and depleted isotopic compositions ($^{87}Sr/^{86}Sr$ 0·70304–0·70308, $^{143}Nd/^{144}Nd$ 0·51306–0·51310, $^{206}Pb/^{204}Pb$ 18·34–18·36), $La_n/Yb_n < 1$, and $Ba_n/Zr_n = 0·55–0·58$ is a result of high-degree melting of a heterogeneous plume source. This source includes primitive relatively undegassed mantle and a refractory and isotopically depleted component different from the North Atlantic N-MORB source. Most of the near-primary mantle-derived rocks in Iceland, including

Kistufell, have chemical characteristics that can be explained by recycling of oceanic lithosphere into the mantle; for example, negative Pb and positive Nb (Ta) anomalies. It is therefore suggested that recycled oceanic lithosphere is a major component of the Iceland mantle plume. This is consistent with HIMU–OIB-like trace element ratios (e.g. K/Nb, La/Nb) observed at Kistufell. The excess Sr and low $\delta^{18}O$ values in Icelandic tholeiites are attributed to isotopically 'depleted' domains of the recycled plume component; more precisely, Sr-rich, hydrothermally altered metagabbroic (and harzburgitic) lower units of recycled oceanic lithosphere. Because the lower units of recycled oceanic lithosphere are expected to be relatively He–Th–U depleted (Moreira & Kurz, 2001), their He isotopic signatures will easily be overprinted by an undegassed lower-mantle component such as FOZO (Hart *et al.*, 1992; Hauri *et al.*, 1994; Hilton *et al.*, 1999).

ACKNOWLEDGEMENTS

This study was partly conducted during my tenure at the NVI, partly during a Ph.D. stipend at the DLC. I wish to thank Karl Grönvold, Niels Oskarsson and Gudmundur Sigvaldason for excellent field guidance in Iceland, analytical support and for enlightening and stimulating discussions. Geochemical data on all nal samples were generated at, or on behalf of, the NVI. All data on samples GEUS 408706–408712 were generated on behalf of the DLC. Karen Bollingberg kindly performed the Mössbauer analysis and Joel Baker the oxygen isotope analysis. I am grateful to Tore Prestvik, Kristján Jonasson, Vesa Nykänen, Rinn Rolfsen, Matti Rossi, and the permanent staff at the NVI and at the Danish Lithosphere Centre (DLC), in particular David Peate and Kent Brooks, for their suggestions, help and inspiration. M. Wilson, S. Revillon, M. Gee, A. Saunders and G. Fitton are thanked for constructive reviews, which considerably improved the manuscript. Peter Roeder is thanked for commenting on an early version of a section on Cr-spinel. NVI is funded by the Nordic Council of Ministers and DLC is funded by the Danish National Research Foundation.

REFERENCES

Anderson, D. L. (2000). The statistics of helium isotopes along the global spreading ridge system and the central limit theorem. *Geophysical Research Letters* **27**, 2401–2404.

Ariskin, A. A. & Nikolaev, G. S. (1996). An empirical model for the calculation of spinel–melt equilibria in mafic igneous systems at atmospheric pressure: 1. Chromian spinels. *Contributions to Mineralogy and Petrology* **123**, 282–292.

Ariskin, A. A., Frenkel, M. Ya., Barmina, G. S. & Nielsen, R. L. (1993). COMAGMAT: a FORTRAN program to model magma differentiation processes. *Computers and Geosciences* **19**, 1155–1170.

Asimov, P. D., Hirschmann, M. M., Ghiorso, M. S., O'Hara, M. J. & Stolper, E. M. (1995). The effect of pressure-induced solid–solid phase transitions on decompression melting of the mantle. *Geochimica et Cosmochimica Acta* **59**, 4489–4506.

Bennett, V. C., Esat, T. M. & Norman, M. D. (1996). Two mantle-plume components in Hawaiian picrites inferred from correlated Os–Pb isotopes. *Nature* **381**, 221–223.

Benoit, M., Polvé, M. & Ceuleneer, M. (1996). Trace element and isotopic characterisation of mafic cumulates in a fossil mantle diapir (Oman ophiolite). *Chemical Geology* **134**, 199–214.

Bernstein, S., Kelemen, P. B. & Brooks, C. K. (1998). Highly depleted spinel harzburgite xenoliths in Tertiary dikes from East Greenland: restites from high degree melting. *Earth and Planetary Science Letters* **154**, 221–235.

Bjarnason, I., Menke, W., Flovenz, O. & Caress, D. (1993). Tomographic image of the spreading center in south Iceland. *Journal of Geophysical Research* **98**, 6607–6622.

Blake, S. (1984). Magma mixing and hybridization processes at the alkalic, silicic, Torfajökull central volcano triggered by tholeiitic Veidivötn fissuring, south Iceland. *Journal of Volcanological and Geothermal Research* **22**, 1–31.

Blundy, J. & Green, T. (2000). A partitioning origin for strontium anomalies in mantle-derived melts. *Journal of Conference Abstracts* **5**, 219.

Bourgeois, O., Dauteuil, O. & Van Vliet-Lanöe, B. (1998). Pleistocene subglacial volcanism in Iceland: tectonic implications. *Earth and Planetary Science Letters* **164**, 165–178.

Breddam, K., Kurz, M. D. & Storey, M. (2000). Mapping out the conduit of the Iceland plume with helium isotopes. *Earth and Planetary Science Letters* **176**, 45–55.

Brodie, J. A. & Fitton, J. G. (1998). Data report: composition of basaltic lavas from the sea-ward dipping reflector sequence recovered during Deep Sea Drilling Project Leg 81 (Hatton Bank). In: Saunders, A. D., Larsen, H. C. & Wise S. W., Jr (eds) *Proceedings of the Ocean Drilling Program, Scientific Results 152*. College Station, TX: Ocean Drilling Progam, pp. 431–435.

Chaffey, D. J., Cliff, R. A. & Wilson, B. M. (1989). Characterisation of the St Helena magma source. In: Saunders, A. D. & Norry, M. J. (eds) *Magmatism in the Ocean Basins. Geological Society, London, Special Publications* **42**, 257–276.

Chauvel, C. & Hemond, C. (2000). Melting of a complete section of recycled oceanic crust: trace element and Pb isotopic evidence from Iceland. *Geochemistry, Geophysics, Geosystems* **1**, 1999GC000002.

Chauvel, C., Goldstein, S. L. & Hofmann, A. W. (1995). Hydration and dehydration of oceanic crust controls Pb evolution in the mantle. *Chemical Geology* **126**, 65–75.

Chen, J. H. & Pallister, J. S. (1981). Lead isotopic studies of the Samail ophiolite, Oman. *Journal of Geophysical Research* **86**, 2699–2708.

Cohen, R. S. & O'Nions, R. K. (1982). The lead, neodymium and strontium isotopic structure of ocean ridge basalts. *Journal of Petrology* **23**, 299–324.

Cohen, R. S., Evensen, N. M., Hamilton, P. J. & O'Nions, R. K. (1980). U–Pb, Sm–Nd and Rb–Sr systematics of mid-ocean ridge basalt glasses. *Nature* **283**, 149–153.

Condomines, M., Grönvold, K., Hooker, P. J., Muehlenbachs, K., O'Nions, R. K., Oskarsson, N. & Oxburgh, E. R. (1983). Helium, oxygen, strontium, and neodymium isotopic relationships in Icelandic volcanics. *Earth and Planetary Science Letters* **66**, 125–136.

Darbyshire, F. A., White, R. S. & Priestly, K. F. (2000). Structure of the crust and uppermost mantle of Iceland from a combined seismic and gravity study. *Earth and Planetary Science Letters* **181**, 409–428.

Davies G. R., Norry, M. J., Gerlach, D. C. & Cliff, R. A. (1989). A combined chemical and Pb–Sr–Nd isotope study of the Azores and Cape Verde hot-spots: the geodynamic implications. In: Saunders, A. D. & Norry, M. J. (eds) *Magmatism in the Ocean Basins. Geological Society, London, Special Publications* **42**, 231–255.

Devey, C. W., Garbe-Schönberg, C.-D., Stoffers, P. Chauvel, C. & Mertz, D. F. (1994). Geochemical effects of dynamic melting beneath ridges: reconciling major and trace element variations in Kolbeinsey (and global) mid-ocean ridge basalt. *Journal of Geophysical Research* **99**, 9077–9095.

Dick, H. & Bullen, T. (1984). Chromian spinel as a petrogenetic indicator in abyssal and alpine peridotites and spatially associated lavas. *Contributions to Mineralogy and Petrology* **86**, 54–76.

Dick, H. J. B., Meyer, P. S., Bloomer, S., Kirby, S., Stakes, D. & Mawer, C. (1991). Lithostratigraphic evolution of *in situ* section of oceanic layer 3. In: Von Herzen, R. P. & Robinson, P. T. (eds) *Proceedings of the Ocean Drilling Program, Scientific Results 118*. College Station, TX: Ocean Drilling Program, pp. 439–540.

Drake, M. J. & Weill, D. F. (1975). The partition of Sr, Ba, Ca, Y, Eu^{3+} and other REE between plagioclase feldspar and magmatic silicate liquid: an experimental study. *Geochimica et Cosmochimica Acta* **39**, 689–712.

Dupré, B. & Allègre, C. J. (1980). Pb–Sr–Nd isotopic correlation and the chemistry of the North Atlantic mantle. *Nature* **286**, 17–22.

Eiler, J. M., Farley, K. A., Valley, J. W., Hofmann, A. W. & Stolper, E. M. (1996). Oxygen isotope constraints on the sources of Hawaiian volcanism. *Earth and Planetary Science Letters* **144**, 453–469.

Elliott, T., Hawkesworth, C. & Grönvold, K. (1991). Dynamic melting of the Iceland plume. *Nature* **351**, 201–206.

Elthon, D. (1983). Isomolar and isostructural pseudo-liquidus phase diagrams for oceanic basalts. *American Mineralogist* **68**, 506–511.

Elthon, D. (1987). Partitioning of Ni between olivine and high-MgO basaltic liquids. *Lunar and Planetary Science Letters* **XVIII**, 258–259.

Elthon, D. (1989). Pressure of origin of primary mid-ocean ridge basalts. In: Saunders, A. D. & Norry, M. J. (eds) *Magmatism in the Ocean Basins. Geological Society, London, Special Publications* **42**, 125–136.

Exley, R. A. (1982). Electron microprobe studies of Iceland Research Drilling Project high-temperature hydrothermal mineral geochemistry. *Journal of Geophysical Research* **87**, 6547–6557.

Eysteinsson, H. & Gunnarsson, K. (1995). Maps of gravity, bathymetry and magnetics for Iceland and surroundings. Orkustofnun OS-95055/JHD-07. Reykjavik: National Energy Authority (internal report).

Falloon, T. J. & Green, D. H. (1987). Anhydrous partial melting of MORB pyrolite and other peridotite compositions at 10 kbar: implications for the origin of primitive MORB glasses. *Mineralogy and Petrology* **37**, 181–219.

Farnetani, D. G. & Richards, M. A. (1995). Thermal entrainment and melting in mantle plumes. *Earth and Planetary Science Letters* **136**, 251–267.

Fitton, J. G., Saunders, A. G., Norry, M. J. & Hardarson, B. S. (1997). Thermal and chemical structure of the Iceland Plume. *Earth and Planetary Science Letters* **153**, 197–208.

Fitton, J. G., Hardarson, B. S., Ellam, R. M. & Rogers, G. (1998*a*). Sr-, Nd-, and Pb-isotopic composition of volcanic rocks from the southeast Greenland margin at 63N: temporal variation in crustal contamination during continental breakup. In: Saunders, A. D., Larsen, H. C. & Wise, S. W., Jr (eds) *Proceedings of the Ocean Drilling Program, Scientific Results 152*. College Station, TX: Ocean Drilling Program, pp. 351–357.

Fitton, J. G., Saunders, A. D., Larsen, L. M., Hardarson, B. S. & Norry, M. J. (1998*b*). Volcanic rocks from the southeast Greenland margin at 63N: composition, petrogenesis and mantle sources. In: Saunders, A. D., Larsen, H. C. & Wise, S. W., Jr (eds) *Proceedings of the Ocean Drilling Program, Scientific Results 152*. College Station, TX: Ocean Drilling Program, pp. 331–350.

Frey, F. A., Walker, N., Stakes, D., Hart, S. R. & Nielsen, R. (1993). Geochemical characteristics of basaltic glasses from the AMAR and FAMOUS axial valleys, Mid-Atlantic Ridge (36°–37°N): petrogenetic implications. *Earth and Planetary Science Letters* **115**, 117–136.

Fujii, T. (1989). Genesis of mid-ocean ridge basalts. In: Saunders, A. D. & Norry, M. J. (eds) *Magmatism in the Ocean Basins. Geological Society, London, Special Publications* **42**, 137–146.

Fujii, T. & Scarfe, C. M. (1985). Composition of liquids coexisting with spinel lherzolite at 10 kbar and the genesis of MORBs. *Contributions to Mineralogy and Petrology* **90**, 18–28.

Furman, T., Frey, F. A. & Park, K.-H. (1991). Chemical constraints on the petrogenesis of mildly alkaline lavas from Vestmannaeyjar, Iceland: the Eldfell (1973) and Surtsey (1963–1967) eruptions. *Contributions to Mineralogy and Petrology* **109**, 19–37.

Furnes, H. (1974). Volume relations between palagonite and authigenic minerals in hyaloclastites, and its bearing on the rate of palagonitization. *Bulletin of Volcanology* **38**, 173–186.

Furnes, H. (1975). Experimental palagonitization of basaltic glasses of varied composition. *Contributions to Mineralogy and Petrology* **50**, 105–113.

Gariepy, C., Ludden, J. & Brooks, C. (1983). Isotopic and trace element constraints on the genesis of the Faeroe lava pile. *Earth and Planetary Science Letters* **63**, 257–272.

Gautason, B. & Muehlenbachs, K. (1998). Oxygen isotopic fluxes associated with high-temperature processes in the rift zones of Iceland. *Chemical Geology* **145**, 275–286.

Gebrande, H., Miller, H. & Einarsson, P. (1980). Seismic structure of Iceland along the RRISP profile. *Journal of Geophysical Research* **47**, 239–249.

Gee, M. A. M., Taylor, R. N., Thirlwall, M. F. & Murton, B. J. (1998*a*). Glacioisostasy controls chemical and isotopic characteristics of tholeiites from the Reykjanes Peninsula, SW Iceland. *Earth and Planetary Science Letters* **164**, 1–5.

Gee, M. A. M., Thirlwall, M. F., Taylor, R. N., Lowry, D. & Murton, B. J. (1998*b*). Crustal processes: major controls on Reykjanes Peninsula lava chemistry, SW Iceland. *Journal of Petrology* **39**, 819–839.

Gerlach, D. C., Stormer, J. C. & Mueller, P. A. (1987). Isotope geochemistry of Fernando de Noronha. *Earth and Planetary Science Letters* **85**, 129–144.

Gerlach, D. C., Cliff, R. A., Davies, G. R., Norry, M. & Hodgson, N. (1988). Magma sources of the Cape Verdes archipelago: isotopic and trace element constraints. *Geochimica et Cosmochimica Acta* **52**, 2979–2992.

Gregory, R. T. & Taylor, H. P., Jr (1981). An oxygen isotope profile in a section of Cretaceous oceanic crust, Samail ophiolite, Oman: evidence for $\delta^{18}O$ buffering of the oceans by deep (>5 km) seawater–hydrothermal circulation at mid-ocean ridges. *Journal of Geophysical Research* **86**, 2737–2755.

Gudmundsson, A. T. (1996). *Volcanoes in Iceland. 10000 Years of Volcanic History*. Reykjavik: Vaka-Helgafell.

Gunnarsson, B., Marsh, B. D. & Taylor, H. P., Jr (1998). Generation of Icelandic rhyolites: silicic lavas from the Torfajökull central volcano. *Journal of Volcanological and Geothermal Research* **83**, 1–45.

Gurenko, A. A. & Chaussidon, M. (1995). Enriched and primitive melts included in olivine from Icelandic tholeiites: origin by continuous melting of a single mantle column. *Geochimica et Cosmochimica Acta* **59**, 2905–2917.

Hanan, B. B. & Schilling, J.-G. (1997). The dynamic evolution of the Iceland mantle plume: the lead isotope perspective. *Earth and Planetary Science Letters* **151**, 43–60.

Hanan, B. B., Blichert-Toft, J., Kingsley, R. & Schilling, J.-G. (2000). Depleted Iceland mantle plume geochemical signature: artifact or multicomponent mixing? *Geochemistry, Geophysics, Geosystems* **1**, 1999GC000009.

Hansen, H. & Grönvold, K. (2000). Plagioclase ultraphyric basalts in Iceland: the mush of the rift. *Journal of Volcanological and Geothermal Research* **98**, 1–32.

Hansteen, T. H. (1991). Multi-stage evolution of the picritic Mælifell rocks, SW Iceland: constraints from mineralogy and inclusions of glass and fluid in olivine. *Contributions to Mineralogy and Petrology* **109**, 225–239.

Hardarson, B. S. & Fitton, J. G. (1991). Increased mantle melting beneath Snaefellsjökull volcano during late Pleistocene deglaciation. *Nature* **353**, 62–64.

Hardarson, B. S., Fitton, J. G., Ellam, R. M. & Pringle, M. S. (1997). Rift relocation—a geochemical and geochronological investigation of a palaeo-rift in northwest Iceland. *Earth and Planetary Science Letters* **153**, 181–196.

Hards, V., Kempton, P. D. & Thompson, R. N. (1995). The heterogeneous Iceland plume: new insights from the alkaline basalts of the Snaefell volcanic centre. *Journal of the Geological Society, London* **152**, 1003–1009.

Hart, S. R. (1988). Heterogeneous mantle domains: signatures, genesis and mixing chronologies. *Earth and Planetary Science Letters* **90**, 273–296.

Hart, S. R. & Davies, K. E. (1978). Nickel partitioning between olivine and silicate melt. *Earth and Planetary Science Letters* **40**, 203–219.

Hart, S. R., Hauri, E. H., Oschmann, L. A. & Whitehead, J. A. (1992). Mantle plumes and entrainment: isotopic evidence. *Science* **256**, 517–520.

Hattori, K. & Muehlenbachs, K. (1982). Oxygen isotope ratios of the Icelandic crust. *Journal of Geophysical Research* **87**, 6559–6565.

Hauri, E. H., Whitehead, J. A. & Hart, S. R. (1994). Fluid dynamics and geochemical aspects of entrainment in mantle plumes. *Journal of Geophysical Research* **99**, 24275–24300.

Hauri, E. H., Lassiter, J. C. & DePaolo, D. J. (1996). Osmium isotope systematics of drilled lavas from Mauna Loa, Hawaii. *Journal of Geophysical Research* **101**, 11793–11806.

Helgason, J. (1989). The Fjallgardar volcanic ridge in NE Iceland: an aborted early stage plate boundary or volcanically dormant zone. In: Saunders, A. D. & Norry, M. J. (eds) *Magmatism in the Ocean Basins. Geological Society, London, Special Publications* **42**, 201–213.

Helgason, Ö. & Steinthorsson, S. (1989). The ferric/ferrous ratio in basalt melts at different oxygen pressures. *Hyperfine Interactions* **45**, 287–294.

Hemond, C., Condomines, M., Fourcarde, S., Allègre, C. J., Oskarsson, N. & Javoy, M. (1988). Thorium, strontium, and oxygen isotopic geochemistry in recent tholeiites from Iceland: crustal influence on mantle-derived magmas. *Earth and Planetary Science Letters* **87**, 273–285.

Hemond, C., Arndt, N. T., Lichtenstein, U. & Hofmann, A. W. (1993). The heterogeneous Iceland plume: Nd–Sr–O isotopes and trace element constraints. *Journal of Geophysical Research* **98**, 15833–15850.

Hess, P. C. (1992). Phase equilibria constraints on the origin of ocean floor basalts. In: Morgan, J. P., Blackman, D. K. & Sinton, J. M. (eds) *Mantle Flow and Melt Generation at Mid-Ocean Ridges. Geophysical Monograph, American Geophysical Union* **71**, 67–102.

Hilton, D. R., Grönvold, K., Macpherson, C. G. & Castillo, P. R. (1999). Extreme $^{3}He/^{4}He$ ratios in northwest Iceland: constraining the common component in mantle plumes. *Earth and Planetary Science Letters* **173**, 53–60.

Hofmann, A. W. (1988). Chemical differentiation of the Earth: the relationship between mantle, continental crust and oceanic crust. *Earth and Planetary Science Letters* **90**, 297–314.

Hofmann, A. W. (1997). Mantle geochemistry: the message from oceanic volcanism. *Nature* **385**, 219–229.

Hofmann, A. W. (1999). The gabbro–harzburgite connection in OIB sources. *EOS Transactions, American Geophysical Union* **V42D-02**, 1182.

Hofmann, A. W. & Jochum, K. P. (1996). Source characteristics derived from very incompatible trace elements in Mauna Loa and Mauna Kea basalts, Hawaii scientific drilling project. *Journal of Geophysical Research* **101**, 11831–11839.

Hofmann, A. W. & White, W. M. (1982). Mantle plumes from ancient oceanic crust. *Earth and Planetary Science Letters* **57**, 421–436.

Hofmann, A. W., Jochum, K. P., Seufert, M. & White, W. M. (1986). Nb and Pb in oceanic basalts: new constraints on mantle evolution. *Earth and Planetary Science Letters* **79**, 33–45.

Ito, E., White, W. M. & Göpel, C. (1987). The O, Sr, Nd and Pb isotope geochemistry of MORB. *Chemical Geology* **62**, 157–176.

Ito, G., Shen, Y., Hirth, G. & Wolfe, C. (1999). Mantle flow, melting, and dehydration of the Iceland mantle plume. *Earth and Planetary Science Letters* **165**, 81–96.

Jakobsson, S. P. (1971). *Palagonitiseringen af tefraen på Surtsey* (English summary). Reykjavik: Museum of Natural Sciences.

Jakobsson, S. P. (1979). Outline of the petrology of Iceland. *Jökull* **29**, 57–73.

Jónasson, K. (1994). Rhyolite volcanism in the Krafla central volcano, north-east Iceland. *Bulletin of Volcanology* **56**, 516–528.

Jakobsson, S. P., Jónsson, J. & Shido, F. (1978). Petrology of the Western Reykjanes Peninsula, Iceland. *Journal of Petrology* **19**, 669–705.

Jull, M. & McKenzie, D. (1996). The effect of deglaciation on mantle melting beneath Iceland. *Journal of Geophysical Research* **101**, 21815–21828.

Kempton, P. D., Hawkesworth, C. J. & Fowler, M. (1991). Geochemistry and isotopic composition of gabbros from layer 3 of the Indian Ocean crust, Hole 735B. In: Von Herzen, R. P. & Robinson, P. T. (eds) *Proceedings of the Ocean Drilling Program, Scientific Results 118*. College Station, TX: Ocean Drilling Program, pp. 127–144.

Kempton, P. D., Fitton, J. G., Saunders, A. D., Nowell, G. M., Taylor, R. N., Hardarson, B. S. & Pearson, G., (2000). The Iceland plume in space and time: a Sr–Nd–Pb–Hf study of the North Atlantic rifted margin. *Earth and Planetary Science Letters* **177**, 255–271.

Kerr, A. C., Saunders, A. D., Tarney, J., Berry, N. H. & Hards, V. L. (1995). Depleted mantle plume geochemical signatures: no paradox for plume theories. *Geology* **23**, 843–846.

Kinzler, R. J. & Grove, T. L. (1992*a*). Primary magmas of mid-ocean ridge basalts 1. Experiments and methods. *Journal of Geophysical Research* **97**, 6885–6906.

Kinzler, R. J. & Grove, T. L. (1992*b*). Primary magmas of mid-ocean ridge basalts 2. Applications. *Journal of Geophysical Research* **97**, 6907–6926.

Kurz, M. D., Jenkins, W. J. & Hart, S. R. (1982). Helium isotopic systematics of oceanic islands and mantle heterogeneity. *Nature* **297**, 43–47.

Kurz, M. D., Meyer, P. S. & Sigurdsson, H. (1985). Helium systematics within the neovolcanic zones of Iceland. *Earth and Planetary Science Letters* **74**, 271–305.

Kystol, J. & Larsen, L. M. (1999). Analytical procedures in the Rock Geochemical Laboratory of the Geological Survey of Denmark and Greenland. *Geology of Greenland Survey Bulletin* **184**, 59–62.

Larsen, G., Gudmundsson, M. T. & Björnsson, H. (1998). Eight centuries of periodic volcanism in the center of the Iceland hotspot revealed by glacier tephrostratigraphy. *Geology* **26**, 943–946.

Lassiter, J. C. & Hauri, E. H. (1998). Osmium isotope variations in Hawaiian lavas: evidence for recycled oceanic lithosphere in the Hawaiian plume. *Earth and Planetary Science Letters* **164**, 483–496.

Leeman, W. P. (1978). Distribution of Mg^{2+} between olivine and silicate melt, and its implications regarding melt structure. *Geochimica et Cosmochimica Acta* **42**, 789–800.

Lundstrom, C. C., Shaw, H. F., Ryerson, F. J., Williams, Q. & Gill, J. (1998). Crystal chemical control of clinopyroxene–melt partitioning in the Di–Ab–An system: implications for element fractionations in the depleted mantle. *Geochimica et Cosmochimica Acta* **62**, 2849–2862.

MacDonald, R., McGarvie, D. W., Pinkerton, H., Smith, R. L. & Palacz, Z. A. (1990). Petrogenetic evolution of the Torfajökull Volcanic Complex, Iceland I. Relationship between the magma types. *Journal of Petrology* **31**, 429–459.

Mäkipää, H. (1978*a*). Mineral equilibria, geothermometers and geobarometers in some Icelandic hyaloclastites. *Bulletin of the Geological Society of Finland* **50**, 113–134.

Mäkipää, H. (1978*b*). Petrological relations in some Icelandic basaltic hyaloclastites. *Bulletin of the Geological Society of Finland* **50**, 81–112.

Mattey, D. P. & Macpherson, C. G. (1993). High-precision oxygen isotope microanalysis of ferromagnesian minerals by laser-fluorination. *Chemical Geology* **105**, 305–318.

McCulloch, M., Gregory, R. T., Wasserburg, G. J. & Taylor, H. P., Jr (1981). Sm–Nd, Rb–Sr and $^{18}O/^{16}O$ isotopic systematics in an oceanic crustal section: evidence from the Samail ophiolite. *Journal of Geophysical Research*, **86**, 2721–2735.

McDonough, W. F. & Sun, S.-s. (1995). The composition of the Earth. *Chemical Geology* **120**, 223–253.

McGarvie, D. (1984). Torfajökull: a volcano dominated by magma mixing. *Geology* **12**, 685–688.

Menke, W. (1999). Crustal isostasy indicates anomalous densities beneath Iceland. *Geophysical Research Letters* **26**, 1215–1218.

Menke, W., Bransdottir, B., Einarsson, P. & Bjarnarson, I. (1996). Reinterpretation of the RRISP-77 Iceland shear-wave profiles. *Geophysical Journal International* **126**, 166–172.

Mertz, D. F. & Haase, K. M. (1997). The radiogenic isotope composition of the high-latitude North Atlantic mantle. *Geology* **25**, 411–414.

Mertz, D. F., Devey, C. W., Todt, W., Stoffers, P. & Hofmann, A. W. (1991). Sr–Nd–Pb isotope evidence against plume asthenosphere mixing north of Iceland. *Earth and Planetary Science Letters* **107**, 243–255.

Meyer, P., Sigurdsson, H. & Schilling, J.-G. (1985). Petrological and geochemical variations along Iceland's neovolcanic zones. *Journal of Geophysical Research* **90**, 10043–10072.

Moreira, M. & Kurz, M. D. (2001). Subducted oceanic lithosphere and the origin of the 'high μ' basalt helium isotopic signature. *Earth and Planetary Science Letters* **189**, 49–57.

Morton, A. C., Dixon, J. E., Fitton, J. G., Macintyre, R. M., Smythe, D. K. & Taylor, P. N. (1988). Early Tertiary volcanic rocks in Well 163/6-1A, Rockall Trough. In: Morton, A. C. & Parson, L. M. (eds) *Early Tertiary Volcanism and the Opening of the NE Atlantic*. *Geological Society, London, Special Publications* **39**, 293–308.

Morton, A. C., Hitchen, K., Ritchie, J. D., Hine, N. M., Whitehouse, M. & Carter, S. G. (1995). Late Cretaceous basalts from Rosemary Bank, Northern Rockall Trough. *Journal of the Geological Society, London* **152**, 947–952.

Muehlenbachs, K., Anderson, A. T., Jr & Sigvaldason, G. E. (1974). Low ^{18}O basalts from Iceland. *Geochimica et Cosmochimica Acta* **38**, 577–588.

Mühe, R., Devey, C. W. & Bohrmann, H. (1993). Isotope and trace element geochemistry of MORB from the Nansen–Gakkel Ridge at 86° north. *Earth and Planetary Science Letters* **120**, 103–109.

Mühe, R., Bohrmann, H., Garbe-Schönberg, D. & Kassens, H. (1997). E-MORB glasses from the Gakkel Ridge (Arctic Ocean) at 87°N: evidence for the Earth's most northerly volcanic activity. *Earth and Planetary Science Letters* **152**, 1–9.

Natland, J. H. (1989). Partial melting of a lithologically heterogeneous mantle: inferences from crystallisation histories of abyssal tholeiites from the Siqueiros Fracture Zone. In: Saunders, A. D. & Norry, M. J. (eds) *Magmatism in the Ocean Basins*. *Geological Society, London, Special Publications* **42**, 41–70.

Neumann, E.-R. & Schilling, J.-G. (1984). Petrology of basalts from the Mohns–Knipovich Ridge; the Norwegian–Greenland Sea. *Contributions to Mineralogy and Petrology* **85**, 209–223.

Nicholson, H. & Latin, D. (1992). Olivine tholeiites from Krafla, Iceland: evidence for variations in melt fraction within a plume. *Journal of Petrology* **33**, 1105–1124.

Nicholson, H., Condomines, M., Fitton, J. G., Fallick, A. E., Grönvold, K. & Rogers, G. (1991). Geochemical and isotopic evidence for crustal assimilation beneath Krafla, Iceland. *Journal of Petrology* **32**, 1005–1020.

Niu, Y. & Batiza, R. (1994). Magmatic processes at a slow spreading ridge segment: 26°S Mid-Atlantic Ridge. *Journal of Geophysical Research* **99**, 19719–19740.

O'Hara, M. J. (1968). Are any ocean floor basalts primary magma? *Nature* **220**, 683–686.

Olafsson, J. & Riley, J. P. (1978). Geochemical studies of the thermal brine from Reykjanes (Iceland). *Chemical Geology* **21**, 219–237.

Oskarsson, N., Sigvaldason, G. E. & Steinthorsson, S. (1982). A dynamic model of rift zone petrogenesis and the regional petrology of Iceland. *Journal of Petrology* **23**, 28–74.

Oskarsson, N., Steinthorsson, S. & Sigvaldason, G. E. (1985). Iceland geochemical anomaly: origin, volcanotectonics, chemical fractionation and isotope evolution of the crust. *Journal of Geophysical Research* **90**, 10011–10025.

Oskarsson, N., Helgason, Ö. & Steinthorsson, S. (1994). Oxidation state of iron in mantle derived magmas of the Icelandic rift zone. *Hyperfine Interactions* **91**, 733–737.

Park, K.-H. (1990). Sr, Nd and Pb isotope studies of ocean island basalts: constraints on their origin and evolution. Ph.D. dissertation, Columbia University, New York, 252 pp.

Presnall, D. C. & Hoover, J. D. (1978). Composition and depth of origin of primary mid-ocean ridge basalts. *Contributions to Mineralogy and Petrology* **87**, 170–178.

Revillon, S., Arndt, N. T., Hallot, E., Kerr, A. C. & Tarney, J. (1999). Petrogenesis of picrites from the Caribbean Plateau and the North Atlantic magmatic province. *Lithos*, **49**, 1–21.

Roeder, P. L. (1982). Experimental study of chromite–basaltic liquid equilibrium. *Proceedings of IAVCEI-IAGC, Generation of Major Basaltic Types, Reykjavik*.

Roeder, P. L. & Emslie, R. F. (1970). Olivine liquid equilibrium. *Contributions to Mineralogy and Petrology* **29**, 275–289.

Roeder, P. L. & Reynolds, I. (1991). Crystallisation of chromite and chromium solubility in basaltic melts. *Journal of Petrology* **32**, 909–934.

Rhodes, J. M. & Hart, S. R. (1995). Episodic trace element and isotopic variations in historical Mauna Loa lavas: implications for magma and plume dynamics. In: Rhodes, M. F. & Lockwood, J. P. (eds) *Mauna Loa Revealed: Structure, Composition, History and Hazards*. *Geophysical Monograph, American Geophysical Union* **92**, 263–288.

Roden, M. F., Frey, F. A. & Clague, D. A. (1994). Geochemistry of tholeiitic and alkalic lavas from the Koolau Range, Oahu, Hawaii: implications for Hawaiian volcanism. *Earth and Planetary Science Letters* **69**, 141–158.

Saunders, A. D., Norry, M. J. & Tarney, J. (1988). Origin of MORB and chemically depleted mantle reservoirs: trace element constraints. *Journal of Petrology, Special Lithosphere Issue* 415–445.

Saunders, A. D., Fitton, J. G., Kerr, A. C., Norry, M. J. & Kent, R. W. (1997). The North Atlantic Igneous Province. In: Mahoney, J.

J. & Coffin, M. F. (eds) *Large Igneous Provinces. Geophysical Monograph, American Geophysical Union* **100**, 45–93.

Schiellerup, H. (1995). Generation and equilibration of olivine tholeiites in the northern rift zone of Iceland. A petrogenetic study of the Bláfjall table mountain. *Journal of Volcanological and Geothermal Research* **65**, 161–179.

Schilling, J.-G., Zajac, M., Evans, R., Johnston, T., White, W., Devine, J. D. & Kingsley, R. (1983). Petrologic and geochemical variations of the Mid-Atlantic Ridge from 29°N to 73°N. *American Journal of Science* **283**, 510–586.

Schilling, J.-G., Kingsley, R., Fontignie, D., Poreda, R. & Xue, S. (1999). Dispersion of the Jan Mayen and Iceland plumes in the Arctic: a He–Pb–Nd–Sr isotope tracer study of basalts from the Kolbeinsey, Mohns and Knipovich Ridges. *Journal of Geophysical Research* **104**, 10543–10569.

Shimizu, N., Hirose, K. & Fei, Y. (1999). Geochemical consequences of partial melting at the core–mantle boundary. *Ninth Annual V. M. Goldschmidt Conference. Lunar and Planetary Institute Contribution* **971**, 272–273.

Shirey, S. B., Bender, J. F. & Langmuir, C. H. (1987). Three-component isotopic heterogeneity near the Oceanographer transform, Mid-Atlantic Ridge. *Nature* **325**, 217–223.

Sigmarsson, O., Hemond, C., Condomines, M., Fourcarde, S. & Oskarsson, N. (1991). Origin of silicic magma in Iceland revealed by Th isotopes. *Geology* **19**, 621–624.

Sigmarsson, O., Condomines, M. & Fourcarde, S. (1992). Mantle and crustal contribution in the genesis of Recent basalts from off-rift zones in Iceland: constraints from Th, Sr and O isotopes. *Earth and Planetary Science Letters* **110**, 149–162.

Sigurdsson, H. (1981). First-order major element variation in basaltic glasses from the Mid-Atlantic Ridge: 29°N to 73°N. *Journal of Geophysical Research* **86**, 9483–9502.

Sigurdsson, H. & Sparks, R. S. J. (1978). Lateral magma flow within rifted Icelandic crust. *Nature* **274**, 126–130.

Sigvaldason, G. E., Annertz, K. & Nilsson, M. (1992). Effect of glacier loading/deloading on volcanism: postglacial volcanic production rate of the Dyngjufjöll area, central Iceland. *Bulletin of Volcanology* **54**, 385–392.

Sims, K. W. W., DePaolo, D. J., Murrell, M. T., Baldridge, W. S., Goldstein, S. J. & Clague, D. (1995). Mechanisms of magma generation beneath Hawaii and mid-ocean ridges: U–Th and Sm–Nd isotopic evidence. *Science* **267**, 508–512.

Slater, L., Jull, M., McKenzie, D. & Grönvold, K. (1998). Deglaciation effects on mantle melting under Iceland: results from the northern volcanic zone. *Earth and Planetary Science Letters* **164**, 151–164.

Slater, L., McKenzie, D., Grönvold, K. & Shimizu, N. (2001). Melt generation and movement beneath Theistareykir, NE Iceland. *Journal of Petrology* **42**, 321–354.

Sobolev, A. V. & Danyushevsky, L. V. (1994). Petrology and geochemistry of boninites from the North Termination of the Tonga Trench: constraints on the generation conditions of primary high-Ca boninite magmas. *Journal of Petrology* **35**, 1183–1211.

Sobolev, A. V., Gurenko, A. A. & Shimizu, N. (1994). Ultra-depleted melts from Iceland: data from melt inclusion studies. *Mineralogical Magazine* **58A**, 860–861.

Sobolev, A. V., Hofmann, A. W., Nikogosian, I. K., Chaussidon, M. & Shimizu, N. (1999). Preservation of local source heterogeneities through convection and remelting. *EOS Transactions, American Geophysical Union* **80**, Fall Meeting Supplement F1171.

Sobolev, A. V., Hofmann, A. W. & Nikogosian, I. K. (2000). Recycled oceanic crust observed in 'ghost plagioclase' within the source of Mauna Loa lavas. *Nature* **404**, 986–990.

Stakes, D. S., Taylor, H. P. & Fisher, R. L. (1984). Oxygen-isotope and geochemical characterisation of hydrothermal alteration in ophiolite complexes and modern oceanic crust. In: Gass, I. G., Lippard, S. J. & Shelton, A. W. (eds) *Ophiolites and Oceanic Lithosphere. Geological Society, London, Special Publications* **13**, 199–214.

Stalder, R., Foley, S. F., Brey, G. P. & Horn, I. (1998). Mineral–aqueous fluid partitioning of trace elements at 900–1200°C and 3·0–5·7 GPa: new experimental data for garnet, clinopyroxene, and rutile, and implications for mantle metasomatism. *Geochimica et Cosmochimica Acta* **62**, 1781–1801.

Staples, R., White, R., Brandsdottir, B., Menke, W., Maguire, P. & McBride, J. (1997). Färoe–Iceland Ridge Experiment, 1, crustal structure of northeastern Iceland. *Journal of Geophysical Research* **102**, 7849–7866.

Staudigel, H., Zindler, A., Hart, S. R., Leslie, T., Chen, C.-Y. & Clague, D. (1984). The isotope systematics of a juvenile intraplate volcano: Pb, Nd and Sr isotope ratios of basalts from Loihi Seamount Volcano, Hawaii. *Earth and Planetary Science Letters* **69**, 13–29.

Stecher, O., Carlson, R. W. & Gunnarsson, B. (1999). Torfajökull: a radiogenic endmember of the Iceland Pb-isotopic array. *Earth and Planetary Science Letters* **165**, 117–127.

Steinthorsson, S., Oskarsson, N. & Sigvaldason, G. E. (1985). Origin of alkali basalts in Iceland: a plate tectonic model. *Journal of Geophysical Research* **90**, 10027–10042.

Stille, P., Unruh, D. M. & Tatsumoto, M. (1986). Pb, Sr, Nd and Hf isotopic constraints on the origin of Hawaiian basalts and evidence for a unique mantle source. *Geochimica et Cosmochimica Acta* **50**, 2303–2319.

Stracke, A., Zindler, A., Blichert-Toft, J., Albarède, F. & McKenzie, D. (1998). Hafnium and strontium measurements in high-MgO basalts from Theistareykir, northern Iceland. *Mineralogical Magazine* **62A**, 1464–1465.

Sun, S.-S. & Jahn, B. (1975). Lead and strontium isotopes in post-glacial basalts from Iceland. *Nature* **255**, 527–530.

Sun, S. S. & McDonough, W. F. (1989). Chemical and isotopic systematics of oceanic basalts: implications for mantle composition and processes. In: Saunders, A. D. & Norry, M. J. (eds) *Magmatism in the Ocean Basins. Geological Society, London, Special Publications* **42**, 313–345.

Sun, S.-S., Tatsumoto, M. & Schilling, J.-G. (1975). Mantle plume mixing along the Reykjanes Ridge axis: lead isotope evidence. *Science* **190**, 143–147.

Sveinbjörnsdottir, A. E., Coleman, M. L. & Yardley, B. J. (1986). Origin and history of hydrothermal fluids of Reykjanes and Krafla geothermal fields, Iceland. *Contributions to Mineralogy and Petrology* **94**, 99–109.

Takahashi, E. & Kushiro, I. (1983). Melting of a dry peridotite at high pressures and basalt magma genesis. *American Mineralogist* **68**, 859–879.

Taylor, R. N., Thirlwall, M. F., Murton, B. J., Hilton, D. R. & Gee, M. A. M. (1997). Isotopic constraints on the influence of the Icelandic plume. *Earth and Planetary Science Letters* **148**, E1–E8.

Thirlwall, M. F. (1995). Generation of the Pb characteristics of the Iceland plume. *Journal of the Geological Society, London* **152**, 991–996.

Thirlwall, M. (2000). Inter-laboratory and other errors in Pb isotope analyses investigated using a ^{207}Pb–^{204}Pb double spike. *Chemical Geology* **163**, 299–322.

Thirlwall, M. F., Gee, M. A. M., Taylor, R. N. & Murton, B. J. (1998). North Atlantic mantle reservoirs: constraints on origins and mixing relations from double-spike Pb isotope data. *Mineral Magazine* **62a**, 1507–1508.

Thirlwall, M., Taylor, R. N., Mattey, D. P., Macpherson, C. G., Gee, M. A. M. & Murton, B. J. (1999). Oxygen isotopic systematics of

Reykjanes mid-ocean ridge basalt: constraints on the origin and the composition of the Icelandic plume mantle. *Ninth Annual V. M. Goldschmidt Conference. Lunar and Planetary Institute Contribution* **971**, 296–297.

Trønnes, R. G. (1990). Basaltic melt evolution of the Hengill volcanic system, SW Iceland, and evidence for clinopyroxene assimilation in primitive tholeiitic magmas. *Journal of Geophysical Research* **95**, 15893–15910.

Valbracht, P. J., Staudigel, H., Honda, M., McDougall, I. & Davies, G. R. (1996). Isotopic tracing of volcanic source regions from Hawaii: decoupling of gaseous from lithophile magma components. *Earth and Planetary Science Letters* **144**, 185–198.

Walker, G. P. L. (1965). Some aspects of Quaternary volcanism in Iceland. *Transactions of Leicester Literary Philosophical Society* **LIX**, 25–39.

Weaver, B. L. (1991). Trace element evidence for the origin of ocean-island basalts. *Geology* **19**, 123–126.

Werner, C.-D. (1997). Data report: geochemistry of rocks and minerals of the gabbro complex from the MARK area. In: Karson, J. A., Cannat, M., Miller, D. J. & Elthon, D. (eds) *Proceedings of the Ocean Drilling Program, Scientific Results 153*. College Station, TX: Ocean Drilling Program, pp. 491–495.

Werner, R. (1994). Struktur und Entstehung subglacialer/sublakustricher Vulkane am Beispiel des Vulkankomplexes Herdubreid/Herdubreidartögl in Island. Ph.D. thesis, Christian Albrechts University, Kiel.

Wiese, P. K. (1992). Geochemistry and geochronology of the Eyjafjoll volcanic system, Iceland. M.Sc. thesis, Oregon State University, Corvallis.

Wolfe, C., Bjarnarson, I. T., VanDecar, J. C. & Solomon, S. C. (1997). Seismic structure of the Iceland mantle plume. *Nature* **385**, 245–247.

Wood, D. A., Joron, J.-L., Treuil, M., Norry, M. & Tarney, J. (1979). Elemental and Sr isotope variations in basic lavas from Iceland and the surrounding ocean floor: the nature of mantle source inhomogeneities. *Contributions to Mineralogy and Petrology* **70**, 319–339.